

# ***Modeling and Analysis for Spent Nuclear Fuel Seismic Testing***

**Spent Fuel and Waste Disposition**

***Prepared for  
US Department of Energy  
Spent Fuel and Waste Science and  
Technology***

**Pacific Northwest National Laboratory**

**Nicholas A. Klymyshyn, Pavlo Ivanusa,  
Casey Spitz, Kevin Kadooka, C.J. Taylor  
Mason, Ben Jensen, Judith A. Bamberger,  
Charlton Campbell, Deborah K. Fagan**

***August 27, 2021***  
**M3SF-21PN010202014**  
**PNNL-31878**

**DISCLAIMER**

This information was prepared as an account of work sponsored by an agency of the U.S. Government. Neither the U.S. Government nor any agency thereof, nor any of their employees, makes any warranty, expressed or implied, or assumes any legal liability or responsibility for the accuracy, completeness, or usefulness, of any information, apparatus, product, or process disclosed, or represents that its use would not infringe privately owned rights. References herein to any specific commercial product, process, or service by trade name, trade mark, manufacturer, or otherwise, does not necessarily constitute or imply its endorsement, recommendation, or favoring by the U.S. Government or any agency thereof. The views and opinions of authors expressed herein do not necessarily state or reflect those of the U.S. Government or any agency thereof.

## SUMMARY

This unlimited distribution report is the deliverable for M3SF-21PN010202014: Modeling and Analysis for Spent Nuclear Fuel Seismic Testing.

This report summarizes the modeling, analysis, and test plan support completed by Pacific Northwest National Laboratory for the spent nuclear fuel dry storage system seismic test plan through May of 2021. Test plan preparation is planned to continue until the seismic test is completed in July of 2022. This report covers preliminary structural dynamic model development and computer-aided design of test hardware.

Based on preliminary modeling, the strongest earthquakes under consideration in this test program provide mechanical loading on the spent nuclear fuel that is comparable to the 30 cm cask drop scenario, although the loads do not appear to be strong enough to cause significant permanent deformation of the fuel assembly spacer grids. The potential for grid deformation during the test will be assessed when the proposed shake table motion becomes available. The weakest earthquakes considered in this test are expected to be comparable to the mechanical loads witnessed in the multimodal transportation test of 2017.

The horizontal canister system is predicted to provide nearly-uniform loading condition on the fuel assemblies it contains, while the vertical cask system is predicted to cause non-uniform dynamic loads on the fuel assemblies. In the horizontal case, gravity keeps the fuel assemblies in contact with one basket wall surface unless the loads are strong enough to cause a separation. In the vertical case, the fuel assemblies are relatively long and slender, and seismic motion in the anticipated test range is predicted to cause the assemblies to lean, tilt, and impact the basket walls throughout the seismic event. These gap closures are a nonlinear force transmission condition, so the vertical system is expected to have more variation and variability than the horizontal system. While the horizontal system is expected to have a relatively more linear response than the vertical system, there is still the potential for nonlinear behavior in the horizontal system because the fuel assemblies are free to slide, bounce, and impact the basket walls if the seismic loads are strong enough.

One major conclusion of this study is that the use of mixed fuel assemblies in the canister will be acceptable. There are differences in overall system response when the mass, center of gravity, or gaps are changed, but the changes in response are within the bounds of a system that contains completely homogeneous fuel assemblies. One important observation is that the loading for each individual fuel assembly within the vertical canister is expected to be different from that of the others because of nonlinearities in the system. The horizontal canister system is expected to have a more uniform and more predictable response than the vertical canister, making variations in fuel assembly characteristics easier to account for.

One important recommendation that comes from this modeling work is to repeat some of the strongest shake tests at different angles, particularly for the vertical cask system. Modeling predicts that strong seismic motion will cause the fuel assemblies to close initial gaps and impact the fuel basket walls when the canister is in the vertical cask configuration. Each shake test will impose a pre-defined three-dimensional time history on the cask system. Repeating the test multiple times is expected to provide somewhat different loadings on the fuel assemblies. Rotating the shake motion about the vertical cask center axis in subsequent tests is expected to be an effective way to change the initial gap conditions, which is needed to explore the full range of mechanical response of the fuel assemblies.

This report also describes progress on PNNL's efforts to develop a crack propagation model to assist in structural dynamic evaluation of welded canisters. This work is more closely related to the cumulative effects of transportation and storage of spent nuclear fuel, but the models developed for the seismic testing are expected to be used as necessary to evaluate the whole canister storage and transportation loading environment. The crack propagation model is developed to take dynamic loading information

from structural dynamic models and calculate the potential growth of an existing crack. The model is calibrated using test data that was collected from PNNL's research on chloride-induced stress corrosion cracking.

## **ACKNOWLEDGEMENTS**

The authors express our sincere thanks to the project's DOE sponsors, Ned Larson and John Orchard for supporting and funding this work.

We also thank Brady Hanson and Steven Ross for their support and contributions to this work, as well as Susan Ennor for technical editing support and Mychailo Toloczko for his help providing crack test data.

We also thank our collaborators on the seismic shake test at Sandia National Laboratories: Elena Kalinina, Doug Ammerman, Sylvia Saltzstein, and Geoff Freeze.

This page is intentionally left blank.

## CONTENTS

SUMMARY .....	iii
ACKNOWLEDGEMENTS .....	v
ACRONYMS .....	xi
1. INTRODUCTION .....	1
2. BACKGROUND/SEISMIC LOADING RANGE .....	3
3. SEISMIC TEST HARDWARE DESIGN .....	7
3.1 Vertical Cask Mockup .....	7
3.2 Dummy Assemblies .....	9
4. EARTHQUAKE MOTION FOR MODEL DEVELOPMENT .....	11
4.1 Columbia Generating Station Working Ground Motion .....	11
4.2 Working Ground Motion Generation Methodology .....	13
4.3 SRS Calculations .....	14
4.4 Optimizing the Signals .....	14
5. CASK FINITE ELEMENT MODELING IN LS-DYNA .....	19
5.1 Vertical Cask System Model .....	19
5.2 Horizontal Cask System Model .....	21
5.2.1 Model Geometry .....	21
5.2.2 ANSYS APDL to LS-DYNA .....	22
5.3 LS-DYNA Modeling Results Summary .....	26
6. FUEL ASSEMBLY MODELING .....	31
6.1 Model Description .....	31
6.2 Initial Modeling Study .....	32
6.2.1 Preliminary Results – Fuel Assembly Dynamics .....	32
6.2.2 Preliminary Results – Fuel Assembly Component Deformation .....	34
6.3 Outlook .....	38
7. TEST CONSIDERATIONS .....	39
7.1 Mixed Fuel Assemblies in the Canister .....	39
7.2 Horizontal Cask Tip-Over Evaluation .....	40
8. CRACK PROPAGATION MODELING .....	43
8.1 Crack Propagation Model Setup .....	43
8.1.1 Crack Propagation Model Calibration .....	46
8.1.2 Example of Model Capabilities .....	48
8.2 Crack Propagation Modeling Summary and Future Work .....	49
9. CONCLUSIONS AND NEXT STEPS .....	51

10. REFERENCES ..... 53

## LIST OF FIGURES

Figure 1.	USGS 2008 Seismic Hazard Map.....	3
Figure 2.	Sample Seismic Hazard Curves (Columbia Generating Station) with the Seismic Test Range Indicated.....	4
Figure 3.	Annual Frequency of Exceedance for Select Time Periods and Probability of Exceedance Levels .....	5
Figure 4.	Vertical Cask Design (Cutaway View).....	7
Figure 5.	Vertical Cask with Canister Inside .....	8
Figure 6.	Doubler Plates Added to Lifting Lugs .....	9
Figure 7.	Preliminary Dummy Assembly Design .....	9
Figure 8.	Peak Ground Acceleration Survey.....	12
Figure 9.	Mean Base Rock Hazard Curves .....	13
Figure 10.	The Frequency Components of the Original and Optimized Signals for an AFE of 1E-5.....	16
Figure 11.	Comparison of Original and Optimized Signals in the Vertical Direction for an AFE of 1E-5 .....	17
Figure 12.	SRS of Optimized Signals for an AFE of 1E-5 .....	18
Figure 13.	Vertical Cask Model .....	20
Figure 14.	Vertical Cask Model with Canister.....	20
Figure 15.	Canister and Contents Mesh .....	21
Figure 16.	NUHOMS® AHSM-HS Used for the Seismic Model .....	22
Figure 17.	ANSYS APDL Volume Plot of the Cask System Model .....	23
Figure 18.	Canister and Support Structure Volumes from ANSYS APLD .....	24
Figure 19.	Element Mesh of the Cask Overpack, Canister Support, and Canister .....	24
Figure 20.	Exterior ANSYS APDL Element Plot .....	25
Figure 21.	Horizontal Cask Model.....	26
Figure 22.	Low Friction Case.....	27
Figure 23.	Cask and Canister Velocity in a Low Friction Case.....	27
Figure 24.	Fuel Assembly Velocity in a Low Friction Case .....	28
Figure 25.	Fuel Assembly Velocity in a 0.5 Friction Case .....	29
Figure 26.	Fuel Assembly Seismic Model. Some parts have been hidden or sectioned for illustrative purposes. ....	31
Figure 27.	Velocity Time History Applied in the Initial Modeling Study.....	32
Figure 28.	Displacement of Bottom Nozzle Relative to Basket Floor.....	33

Figure 29.	Top and Bottom Nozzle (left) and Representative Fuel Rod (right) Resultant Acceleration .....	33
Figure 30.	Fuel Rod and Guide Tube Peak Strains .....	35
Figure 31.	Peak and Average Fuel Rod and Guide Tube Strains as a Function of Elevation .....	36
Figure 32.	Peak Fuel Rod and Guide Tube Accelerations as a Function of Elevation and Time .....	37
Figure 33.	Grid Deformation in Both Lateral Directions (X and Y) in the Uppermost Grids (1 and 2) and Lowermost Grid (10) .....	38
Figure 34.	Fuel Response in a Vertical Canister: Balanced (Left) and Unbalanced (right) .....	40
Figure 35.	Fuel Assembly Seismic Response in Horizontal Cask System .....	41
Figure 36.	Schematic of a Cylindrical Fatigue Specimen Used in this Model. Where a is crack depth and D is the diameter of the gauge section of the specimen.....	45
Figure 37.	Crack Growth Rate as a Function of Stress Intensity Factor Range for a Material. This is categorized into three stages of crack growth, small crack growth, and long crack growth and unstable crack growth.....	46
Figure 38.	Comparison between the Model and Experiments (Vasek et al. 2003) for Small Crack Growth Rate as a Function of Crack Length for SS316 .....	47
Figure 39.	da/dn vs. $\Delta K$ Curves Used to Calibrate the Long Crack Growth Portion of the Model for A) SS316 (Sajith et al. 2019) and B) SS304.....	47
Figure 40.	A S-N Curve Comparison between Experimental and Crack Propagation Model Prediction for A) SS316 and B) SS304. The arrows indicate infinite fatigue life. ....	48
Figure 41.	Crack Propagation Model Prediction for Two Different Loading Conditions for SS316. A) Crack length as a function of cycles for the Variable 1 loading condition. B) Crack length as a function of cycles for the Variable 2 loading condition. C) Stress intensity range as a function of cycles for the Variable 1 loading condition. D) Stress intensity range as a function of cycles for the Variable 2 loading condition. ....	49

## **ACRONYMS**

AFE	annual frequency of exceedance
AHSM-HS	Advanced Horizontal Storage Module- High Seismic
ANL	Argonne National Laboratory
APDL	Ansys Parametric Design Language
CURIE	Centralized Used Fuel Resource for Information Exchange
FFT	Fast Fourier Transform
ISFSI	independent spent fuel storage installation
LC	long crack
LHPOST	Large High Performance Outdoor Shake Table
MMTT	Multi-Modal Transportation Test
MPC	multipurpose canister
NUHOMS <sup>®</sup>	NUTECH HORIZONTAL MODULAR Storage
PGA	peak ground acceleration
PNNL	Pacific Northwest National Laboratory
PWR	pressurized-water reactor
SC	short crack
SDOF	single degree of freedom
SFWST	Spent Fuel and Waste Science and Technology
SNF	spent nuclear fuel
SNL	Sandia National Laboratories
SRS	shock response spectra
US	United States
USGS	United States Geological Survey

This page is intentionally left blank.

# MODELING AND ANALYSIS FOR SPENT NUCLEAR FUEL SEISMIC TESTING

## 1. INTRODUCTION

The U.S. Department of Energy's Spent Fuel and Waste Science and Technology (SFWST) program is working to close the stress profiles knowledge gap for spent nuclear fuel (SNF). This knowledge gap refers to the stress, strain, and mechanical loading that are anticipated to occur during normal conditions of SNF transportation and storage. The SFWST program recently completed physical tests that measured the dynamic response of nuclear fuel assemblies during transportation (McConnell et al. 2018; Kalinina et al. 2018; Klymyshyn et al. 2018) and 30 cm package drop scenarios (Kalinina et al. 2020; Klymyshyn et al. 2020a). The SFWST program now has access to excess SNF dry storage canisters and is planning to use one to measure the shock and vibration response of nuclear fuel rods and fuel assembly components in a test planned to take place using the University of California–San Diego Large High Performance Outdoor Shake Table (LHPOST) facility in San Diego. Pacific Northwest National Laboratory's (PNNL's) role on the test team is to use modeling and analysis to help define the test plan. This report covers modeling and analysis topics, as well as some computer-aided design of test components.

Section 2 discusses the background related to defining the seismic loading range for the test. Earthquakes are random occurrences and the seismic hazard is defined using probabilistic concepts. As planned, the test will include the relatively strong design basis seismic loading range, which reflects the safety inherent in SNF systems, but means the test range will include relatively low probability loading scenarios.

Section 3 presents progress made on the design of hardware for the test. One key system is a mockup vertical cask system that can hold a NUTECH Horizontal Modular Storage (NUHOMS<sup>®</sup>) canister, enabling the test to collect data about both horizontal and vertical systems. Another important component is the dummy assembly design that will be used in most of the 32 fuel assembly locations at which the hardware will be used. We currently expect three to four surrogate instrumented fuel assemblies will be used in the test, so the remaining fuel assembly locations will need dummy assemblies. Both design efforts are progressing, and the designs are expected to be finalized at a time closer to the test date.

The PNNL modeling team needed ground motions to use when developing the finite element models of the cask systems to be studied during the test. SC Solutions is responsible for providing the final ground motions and shake table inputs to be used in the test. Section 4 describes the development of temporary ground motion by PNNL for use in model development until the SC Solutions seismic conditions are provided.

Section 5 describes the current state of the cask-level finite element models. These models calculate the seismic response of a single vertical or horizontal SNF cask system on a section of concrete pad. Both versions of the cask (vertical and horizontal) contain a canister, which has appropriate freedom of motion inside the cask. Within the canister is a basket structure with 32 rectangular fuel assemblies with dimensions consistent with those of pressurized-water reactor (PWR) fuel assemblies. Preliminary seismic analyses are presented that use the ground motion described in Section 4.

The preliminary seismic response from the vertical cask system described in Section 5 was used to calculate the response of a detailed fuel assembly. The basket motion calculated in the cask-level model was used as the dynamic loading conditions for the fuel assembly-level model. Section 6 describes the calculated mechanical response of the fuel assembly.

Section 7 discusses three key technical topics where modeling is needed to inform the test plan. The intent to use a mix of different fuel assemblies with different mass and envelope size was investigated. The need to brace the horizontal cask system against tipping was studied. The need to brace the canister open lid during testing was considered, but not yet evaluated. Initial results are reported where available, but in

all cases a final determination must wait until we have the shake table motion that will be proposed by SC Solutions.

Section 8 describes the progress made on a crack propagation modeling effort that is related to seismic modeling but is not directly related to the shake test plan. The crack modeling work is related to extracting structural dynamic loading information from models of SNF canisters (the kind described in Section 5) and determining whether an existing crack would grow larger from the calculated loading history. The shake test will not study or evaluate canister integrity, but the finite element models developed for the shake test are useful for that purpose.

The conclusions and next steps are discussed in Section 9. Much of the modeling work needs to be updated when shake table motion is provided by SC Solutions. The preliminary results suggest that the vertical cask configuration will provide significant, non-uniform mechanical loading to the SNF. The magnitude of cladding strain in the strongest earthquake scenario is expected to be similar to the 30 cm fuel assembly drop tests, although grid buckling is not expected. There remains some concern about the potential for grid permanent deformation, but more detailed analysis using the proposed shake table motion is needed to make a final prediction.

## 2. BACKGROUND/SEISMIC LOADING RANGE

One of the key fundamental principles of the seismic phenomenon is that earthquakes are unpredictable, random occurrences. The seismic hazard for a location is defined in probabilistic terms. Stronger earthquakes are generally less likely than weaker earthquakes. Structural engineers design structures to withstand a certain earthquake intensity, with the idea that a structure will survive an earthquake up to its chosen design basis. If an earthquake occurs that is stronger than the design basis, then there is no guarantee that the structure will survive. One of the first decisions the test team needed to make was what range of earthquakes would be used for the test.

To help explain the seismic hazard, Figure 1 shows the 2008 seismic hazard map from the United States Geological Survey (USGS) (Peterson et al. 2008). The contour colors indicate peak ground acceleration ranges (in % g) for all of the United States (US). These values are defined based on a 2% probability of exceedance within a 50-year time period, which means that 98% of earthquakes that are anticipated to occur in 50 years are expected to be within or below the contour values. The remaining 2% of earthquakes are expected to exceed the contour values. Hazard maps like this can be constructed for any choice of time period and probability of exceedance. The time period and probability of exceedance to be used are key decisions for defining the seismic test.

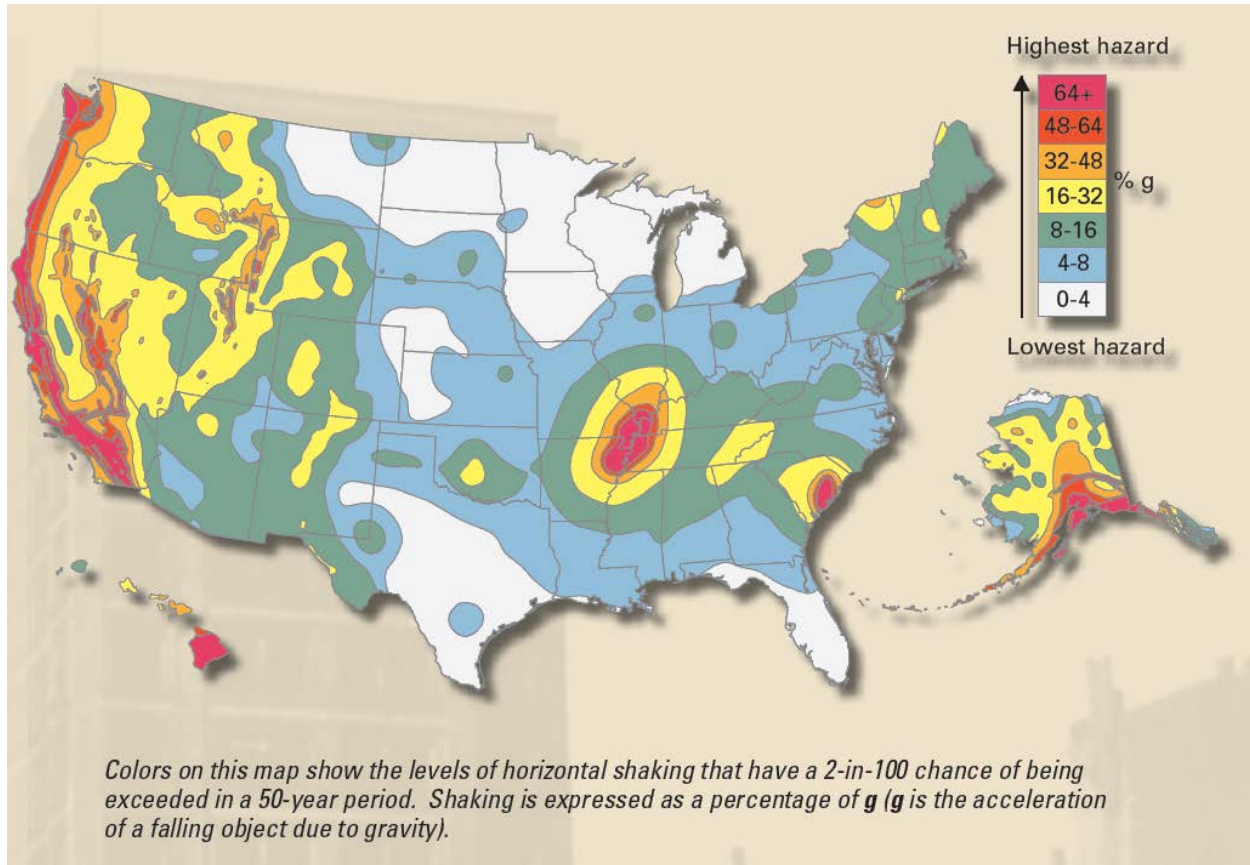


**Figure 1. USGS 2008 Seismic Hazard Map**

The time period of interest for this test campaign was selected to be 50 to 300 years, to be consistent with the cumulative effects framework proposed by Klymyshyn et al. (2020b). The cumulative effects framework considers the uncertain SNF dry storage timeframe in 50-year increments: 50, 100, 150, 200, 250, and 300 years. The concept of cumulative effects considers all of the relatively small mechanical loads, thermal loads, material degradation, and other phenomena that could affect SNF throughout the full

lifecycle—from the time the SNF enters dry storage until its final disposition. This lifecycle could include multiple transportation events and multiple storage locations over a relatively long period of time. The seismic shake test is intended to provide model validation data for fuel assembly, canister, and cask-level structural dynamic models that will eventually be used in cumulative effects analysis.

The probability of exceedance is an important concept in seismic engineering, but it is most often represented as the annual frequency of exceedance (AFE). In AFE, the probability of exceedance is normalized to a 1-year time period. Figure 2 shows an example of how AFE is used to represent the seismic hazard for the Columbia Nuclear Generating Station (Swank 2015). The vertical axis is AFE, which is the probability that an earthquake of that magnitude will be exceeded in 1 year. The highest AFE value on the chart is 1E-2, which means there is a 1% probability that the earthquake motion will be exceeded in any 1 year period. The lowest AFE is 1E-8, which means there is a 1 in 100 million chance that the earthquake motion will be exceeded in any given year. The curves in Figure 2 are used to construct the earthquake frequency spectrum for any value of AFE.

Another way to think of AFE is with its reciprocal—the return period. An AFE of 1E-5 is equal to a return period of 100,000 years. In general terms, the AFE of 1E-5 represents an earthquake that is only expected to occur every 100,000 years. The probability of a 100,000-year earthquake happening in any 1 year is very low.

Some nuclear power plants and independent spent fuel storage installations (ISFSIs) in the US have an AFE = 1E-5 design basis, so that was chosen as the top end of testing to ensure it covered the design basis for all US SNF casks. AFE = 1E-3 was selected as the low end of testing to give two full orders of magnitude of spread. Figure 2 shows an example of a seismic hazard map with the AFE ranges color-coded. The orange and green color bands are the test range (AFE = 1E-3 to 1E-5). The blue and red bands exist on the seismic hazard map but are too weak to test and too strong to be relevant, respectively.

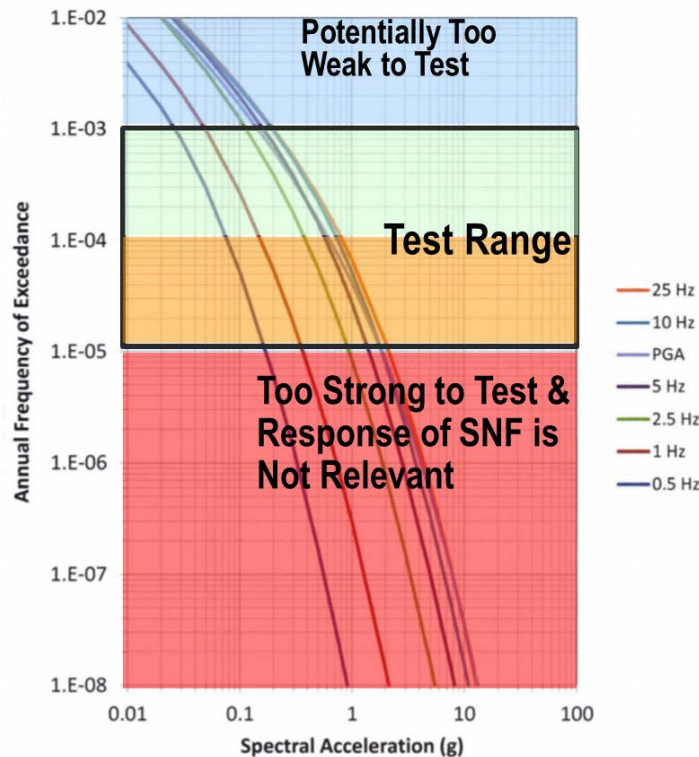


**Figure 2. Sample Seismic Hazard Curves (Columbia Generating Station) with the Seismic Test Range Indicated**

It is useful to consider the probability of exceedance for this test because the goal of the program is to understand the mechanical loading conditions applied to SNF. Figure 3 shows the AFE values that correspond to a range of time durations and probabilities of exceedance. The color coding is consistent with Figure 2. The green and orange cells are in the seismic test plan range and they are in the relatively low probability of exceedance range (16%, 2%, 0.3%). One observation about this figure is that the test is focused on the relatively low probability seismic events. The 50% probability of exceedance (even odds, a coin flip) is in the white and blue cells, and these hypothetical earthquake amplitudes are too small to test. While the testing should provide insight into the highest reasonable loads applied to SNF, we will also have to consider the probability of those mechanical loads occurring and the potential for a practical impact on the SNF storage and transportation lifecycle.

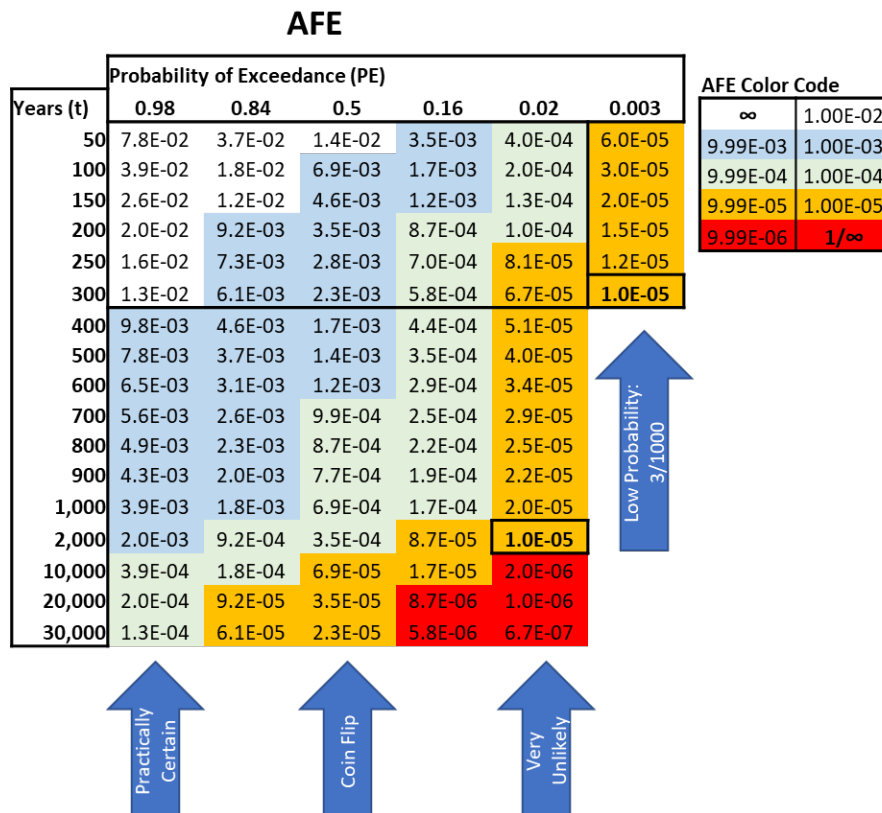


**Figure 3. Annual Frequency of Exceedance for Select Time Periods and Probability of Exceedance Levels**

In summary, this discussion of earthquake magnitudes and probabilities informed the formulation of the test plan. According to the plan, SC Solutions is responsible for defining the earthquake free-field motions to be represented in the test. SC Solutions is also responsible for proposing the shake table inputs based on free-field ground motions and soil structure interaction, along with input from the test team. PNNL's finite element models will be validated with the test data, so the anticipated range of validated models is in the 1E-3 to 1E-5 AFE range. As is discussed in Section 6, we are estimating the 1E-5 AFE range to be comparable to the 30 cm cask drop scenario in terms of the mechanical load it imparts to the SNF (although grid permanent deformation is not predicted during seismic loading conditions). The dynamic response at the bottom end of the test range is not yet estimated, but we can assume that the higher AFE values will trend toward negligible mechanical loading as the earthquake strength decreases. Establishing at what loading the seismic response is negligible will be an important step in understanding the loading range and in closing the knowledge gap.

This page is intentionally left blank.

### 3. SEISMIC TEST HARDWARE DESIGN

PNNL assisted with the design of two key pieces of test hardware: the vertical cask system and the dummy assemblies. In both cases, it was important to create engineering drawings that could be used to acquire fabrication bids.

#### 3.1 Vertical Cask Mockup

The vertical cask mockup system was designed to be similar to other vertical concrete cask systems used by the industry. A rendering of the cask with a cutaway view of the interior is shown in Figure 4. Figure 5 shows the cask with an SNF canister inside. A key design feature that is visible in both figures is the hole in the pedestal to accommodate the grapple ring on the NUHOMS® canister. Most of the cost of fabricating the cask is expected to be in welding the components of the steel structure together to serve as an inner and bottom form for pouring concrete. The outer shell of the cask is envisioned to be an outer steel form that is provided by the concrete supplier. The outer form would stay in place during the test to keep the concrete from spalling off during the shake table testing.

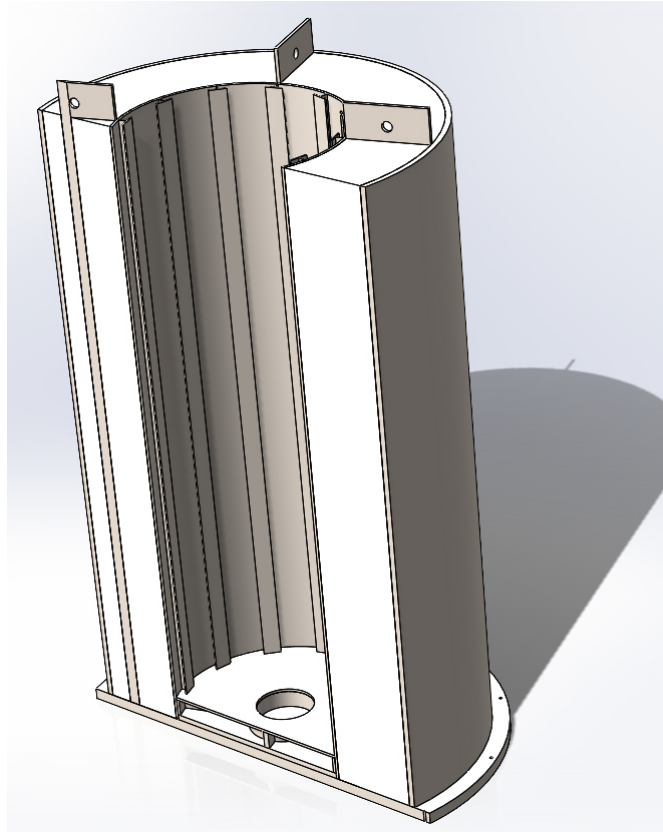
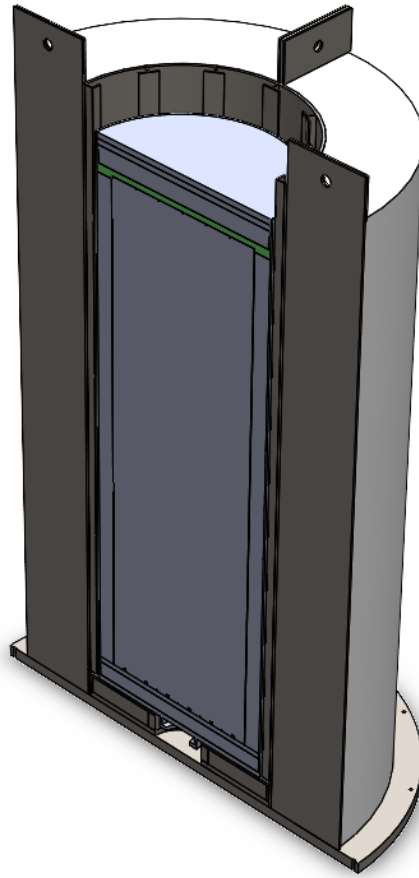


Figure 4. Vertical Cask Design (Cutaway View)



**Figure 5. Vertical Cask with Canister Inside**

One design feature visible in Figure 4 and Figure 5 that still needs to be changed is the base plate, which is wider than the rest of the cask and has holes for anchor bolts. This feature will be redesigned to allow for anchoring during the test, but it will be kept at the correct diameter at the bottom so the footprint of the cask is the same as that of other casks in the US inventory. Having the base plate be wider than the cask raises concerns that the test article would be too resistant to rocking and rolling during strong earthquakes.

Analysis was also performed to ensure the lifting lugs are adequate for lifting the full weight of the loaded cask, which is expected to be equal to or less than 360,000 lb. Doubler plates were added in the first design revision to ensure that the load could be supported by two of the four lugs. The final design of the lifting lug region is shown in Figure 6.

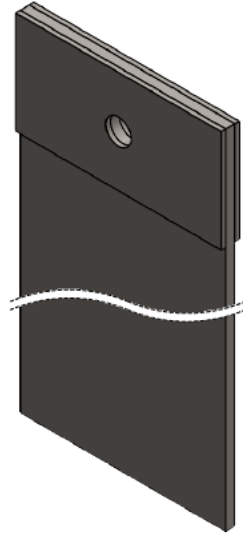


**Figure 6. Doubler Plates Added to Lifting Lugs**

### **3.2 Dummy Assemblies**

PNNL recently began designing a dummy assembly for use in the seismic test. The first preliminary dummy fuel assembly design is shown in Figure 7. Important design considerations are cost and ease of construction. A standard 7-inch-wide square steel channel is used as the base structure. Inside the steel channel is concrete for mass. Teflon pads are used on the outside surfaces of the steel channel to achieve a desired gap between the dummy assembly and the fuel basket. A central rod and rebar structure runs down the center of the channel, and one end has a threaded hole to allow a lifting hook to be attached. This current design will be finalized with the test team over the next month or two.



**Figure 7. Preliminary Dummy Assembly Design**

This page is intentionally left blank.

## 4. EARTHQUAKE MOTION FOR MODEL DEVELOPMENT

Developing the shake table motions for use in the cask tests is a complex task. SC Solutions was contracted to complete the task in two phases. The first phase is to create a set of free-field ground motions that are representative of earthquake ground motion at hypothetical locations throughout the US where SNF ISFSIs might be. The second step is to perform soil-structure interaction analyses to provide shake table motions that account for various soil conditions. The first phase is due to be complete in August 2021. The second is due to be complete some months later. In the interim, PNNL developed an example earthquake ground motion to test the finite element models of the cask systems while SC Solutions completed their work.

This section describes the numerical fitting methods that PNNL used to generate the example ground motion. The steps were to a) choose a hazard spectrum, b) search a limited database of historical earthquake ground motion data to find the best match, and c) modify the ground motion in the frequency domain to achieve an acceptable degree of fit to the target spectrum. PNNL's data fitting methods are described here to provide context to the model results reported in Section 5.3, but they may not be consistent with standard seismic engineering methods. The example seismic acceleration history simulates relatively strong ground motion, which is sufficient until it is replaced by the input data from SC Solutions. We do not propose to use the methodology described here for any other purposes.

The goal of this methodology is to generate ground motion that approximates a seismic hazard level at an arbitrary location. The hazard spectra for the Columbia Generating Station were selected as an example, but we are not attempting to model the seismic conditions at that specific location. A site-specific seismic cask analysis requires knowledge of the soil or rock conditions below a pad to translate free-field ground motion into pad motion to account for soil-structure interaction. Our analyses assume that the free-field ground motion is equal to the pad motion, which is a reasonable assumption at hard rock sites where soil-structure interaction is negligible but may underpredict pad motion at sites classified as soft rock or soil. While the methodology aims for ground motion that is similar to the 1E-5 hazard level at the Columbia Generating Station, it would take a detailed site-specific analysis to determine how well the example ground motion approximates the ISFSI pad motion at the 1E-5 hazard level.

### 4.1 Columbia Generating Station Working Ground Motion

PNNL performed a brief survey of freely available information about the seismic hazard at nuclear power plant and ISFSI sites in the US. While many parameters are needed to define earthquakes, the peak ground acceleration (PGA) was used as a primary parameter. PGA is the maximum acceleration at ground level and it is often useful to think of it as a threshold—accelerations will be equal to or lower than the PGA.

Figure 8 is a map that summarizes PNNL's seismic hazard survey. The underlying map is a U.S. Nuclear Regulatory Commission (NRC) graphic that shows ISFSIs in the US (NRC 2020). PNNL circled selected locations where publicly available seismic hazard information was reviewed. For example, the Columbia Generating Station information came from a letter from the power plant operator to NRC, in the time period following the Fukushima Daiichi accident of 2011 (Swank 2015). Similar information for all US nuclear power plants is publicly available. Note that the survey was not comprehensive and was only intended to gather a high-level understanding of the seismic hazard in the different regions of the US. The Columbia Generating Station in southeastern Washington State was chosen as the basis for creating working ground motions because it had the highest PGA of the sites investigated. Relatively strong ground motion is needed to exercise the nonlinear contact features of the model.

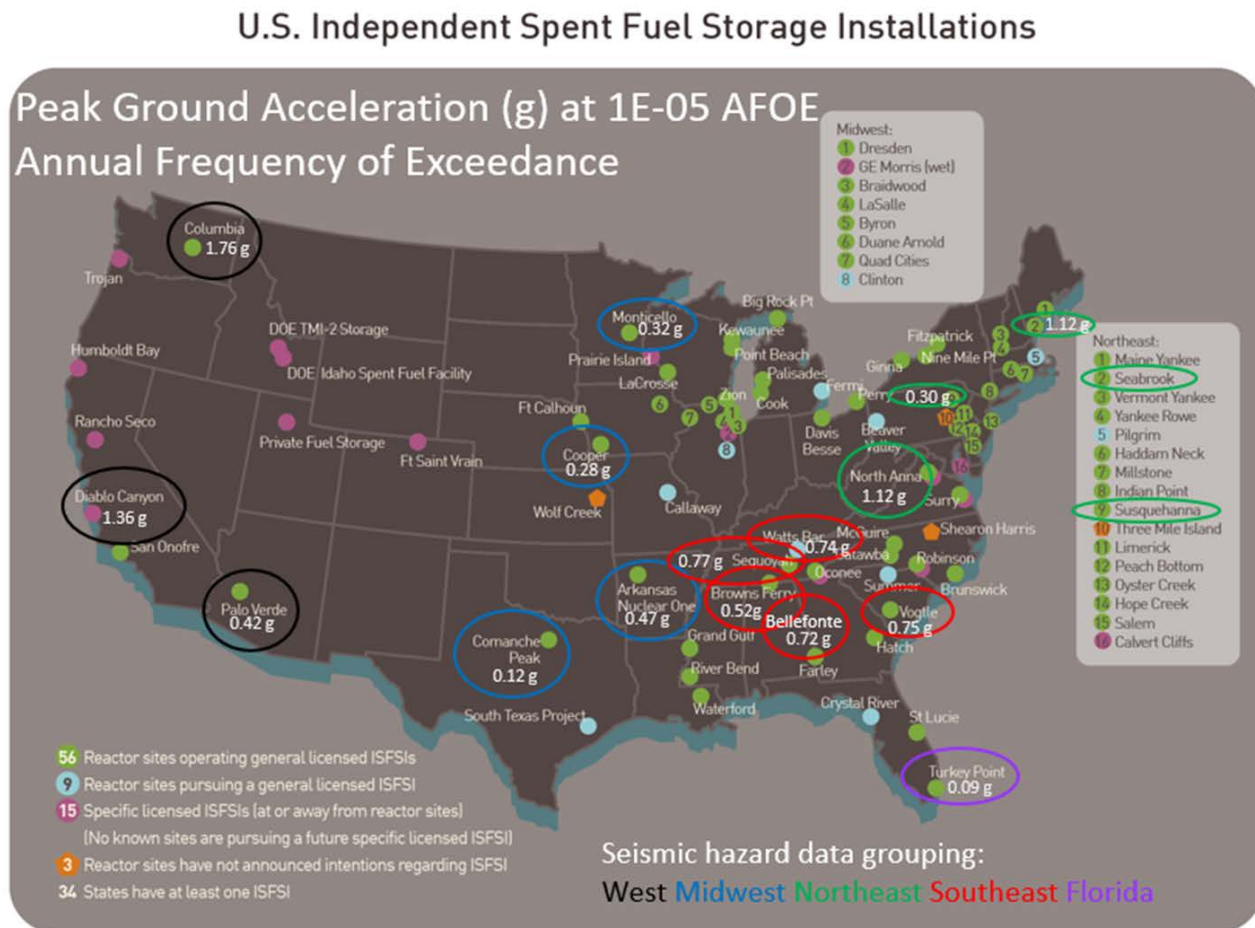


**Figure 8. Peak Ground Acceleration Survey**

The seismic hazard curves for the Columbia Generating Station are shown in Figure 9. These curves represent the earthquake hazard at the base rock level, which is typically below layers of soil. A seismic analysis of a structure would consider how the depth and specific layers of soil affect the transmission of base rock motions to the structure. For the purposes of generating working ground motion, the soil effects are neglected. This simplification can be thought of as a case where the ISFSI sits directly on hard rock. Real ISFSIs are typically situated on layers of prepared substrate, so we are expecting that the working ground motion we generated for model development will differ from the final motions to be provided by SC Solutions, but it is not known how significant the differences will be.

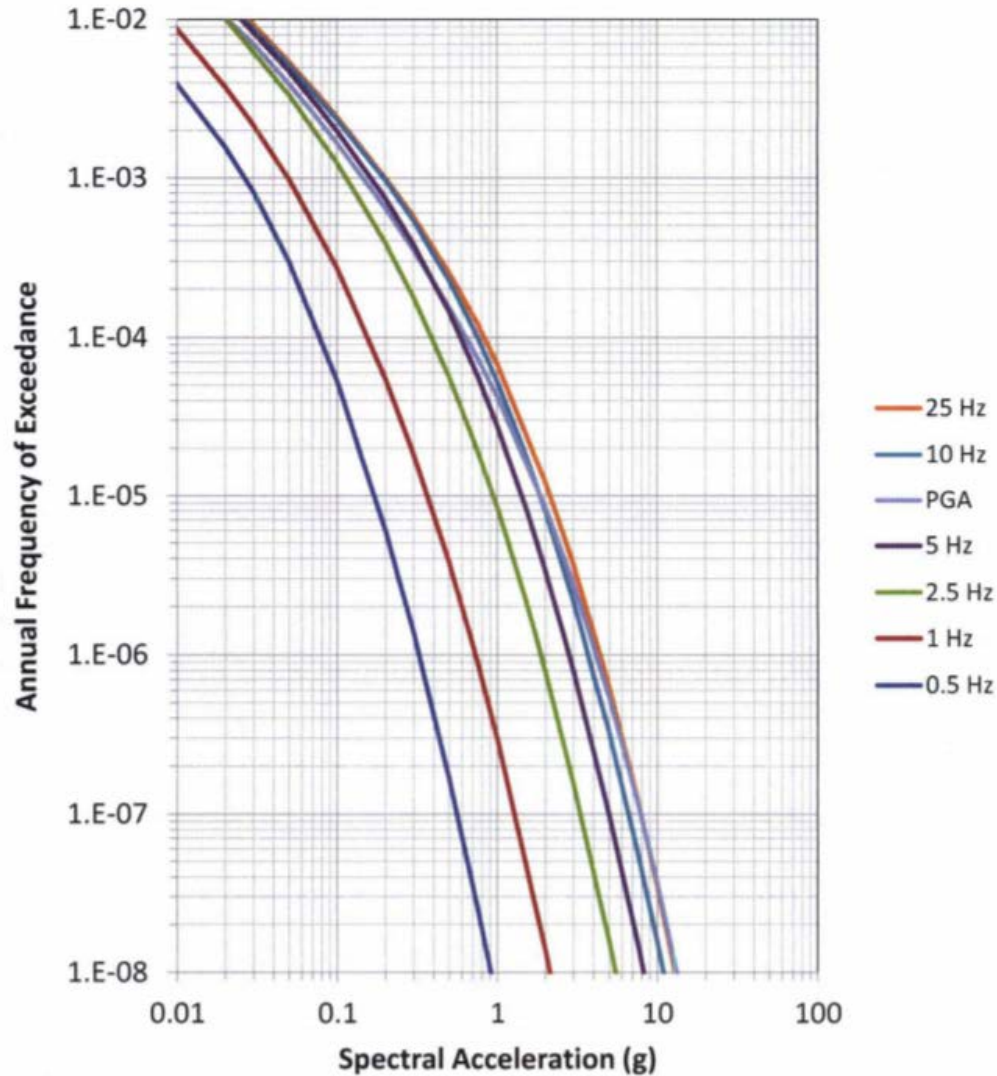


Figure 9. Mean Base Rock Hazard Curves

## 4.2 Working Ground Motion Generation Methodology

The working ground motions were generated from the Columbia Generating Station base rock hazard curves and a database of hundreds of historical ground motion recordings. The problem was cast as an optimization problem, where a target earthquake spectrum was proposed, and the database of earthquakes was searched to find the best match. In optimization problem terms, the error between the target and the candidate earthquake motion was minimized. Once the best match was identified, the characteristics of the candidate earthquake were modified as little as possible to achieve a best fit with the target earthquake spectrum. This process created hypothetical ground motion at the strongest earthquake level that will be considered in this test campaign (1E-5 AFE). This section describes the process details.

Last year (2020), PNNL downloaded hundreds of historical earthquake time histories from the USGS of various magnitudes and locations across the US. This year, the shock response spectra (SRS) of each earthquake time history in the database was calculated. These SRS were then compared to ideal values at each AFE, producing an overall error. The AFE values were 1E-2 to 1E-6 at integer powers of 10. An additional AFE at 1.5E-4 was also analyzed.

### 4.3 SRS Calculations

SRS calculations utilized the maximum absolute value (maximax) of the acceleration response spectra as defined in ISO 18431-4:2007(E). This SRS calculation uses the maximum absolute value of the input data to produce the resultant spectra. The resultant spectra show the expected magnitude of the response of a single degree of freedom (SDOF) system to an input pulse as a function of natural frequency. The SDOF system is assumed to have a damping coefficient of 5%. Error associated with the calculation (based on input data recording frequency and the maximum search function) was also determined. For each earthquake, the SRS calculation was performed for an east-west component, a north-south component, and a vertical component.

### 4.4 Optimizing the Signals

Once SRS values were found for each earthquake in the database, the SRS values were compared to the AFE values for the Columbia Generating Station. The magnitude of the response associated with each AFE was compared to the corresponding target frequencies in the SRS data. (The target frequencies are the ones specified in the seismic hazard, which in this case are the labeled curves in Figure 2.)

Furthermore, the error at each frequency was used to weight the differences. The overall goodness of fit was determined using the weighted root mean square error (wRMSE) calculation determined as follows:

$$wRMSE = \sqrt{\frac{\sum_{i=1}^n (AFE_i - SRS_i)^2 / \Delta_{SRS,i}}{\sum_{i=1}^n 1 / \Delta_{SRS,i}}}$$

where  $AFE_i$  is the magnitude of the AFE acceleration at frequency  $i$ ,  $SRS_i$  is the magnitude of the SRS at frequency  $i$ , and  $\Delta_{SRS,i}$  is the error in the SRS at frequency  $i$ .

The earthquakes with the lowest error in each direction (east-west, north-south, and vertical) for each AFE were selected. Then these earthquakes were run through an optimization algorithm to decrease the SRS error at the six target frequencies for the Columbia Generating Station: 0.5, 1, 2.5, 5, 10, and 25 Hz.

The procedure for optimizing the signals included the following steps:

1. The signals were up-sampled to 100 Hz if the sample frequency was lower than 100 Hz to ensure that the three directions had the same time length. Up-sampling was also chosen over down-sampling to avoid any instances of aliasing. The up-sampling was performed using a spline fit to avoid introduction of spurious high-frequency noise.
2. The signal lengths were reduced to the 5 seconds around the earthquake peak. These 5 seconds were chosen with two different methods, depending on the earthquake. The first method was to find the highest acceleration magnitude and then take a centered 5-second period around that peak. If the peak, however, was less than 2.5 seconds after the start of the signal, the 5-second period would start at the beginning of the signal. The second method was just a fixed starting point. This method was used to avoid signals where a majority of the 2.5 seconds before the peak showed essentially zero acceleration.
3. The signals were converted into frequency space using the Fast Fourier Transform (FFT) algorithm in Matlab.
4. In frequency space, the frequency amplitudes around the six target frequencies for the Columbia Generating Station were either amplified or diminished to reduce the overall SRS error. The frequency width ranged between 0.2 and 1 Hz around the important frequencies depending on the earthquake.
5. The signals were then converted back into time histories using an inverse FFT algorithm.

6. The optimized signals in each direction were then combined into an overall signal using with two horizontal directions and one vertical direction. In the resultant signal, the X direction was the horizontal component, either east-west or north-south, with the larger acceleration magnitude. The Y direction was the horizontal component with the smaller acceleration magnitude. The Z direction was always the vertical component.

Example results are shown in the figures below to demonstrate the effects of the optimization calculation. Figure 10 shows an example of the original and optimized FFTs, Figure 11 shows the original and optimized acceleration time histories,<sup>1</sup> and Figure 12 shows the SRS curves for all three directions for an AFE of 1E-5. The FFT figure shows that the optimization did not affect the majority of the frequencies, only those select few mentioned previously. In this example, the acceleration time history was also not dramatically changed, but the addition of higher frequencies did produce some higher peaks than the original signal.

An important point to consider when looking at these example results is that the frequency content was deliberately under-optimized around 25 Hz for several reasons. First, the higher frequencies have a much lower impact on the total SRS error, and thus optimizing the SRS error around the lower frequencies took precedence. Second, optimizing the frequency content around 25 Hz caused the acceleration time history to have significantly larger peaks than the original values in many earthquakes, which may incorrectly skew modeling results. Third, even though the optimization algorithm up-sampled signals to 100 Hz, many of these signals were recorded at 50 Hz, so the amplitudes around 25 Hz may have some artifacts from the up-sampling.

The preliminary ground motions generated using this methodology are being used for model development and test planning only. The ground motions from SC Solutions will be implemented when received.

---

<sup>1</sup> The times in this figure are not necessarily the absolute times of the original signal. They are just the 5-second signal used for analysis.

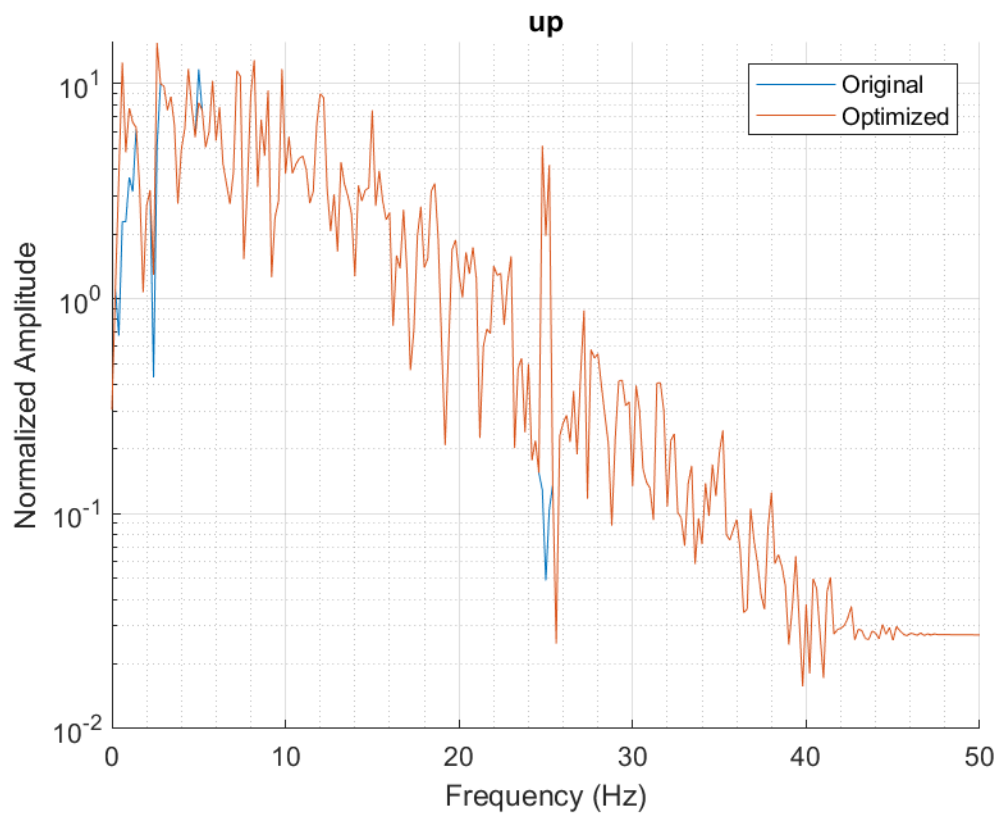


**Figure 10. The Frequency Components of the Original and Optimized Signals for an AFE of  $1E-5$ .**

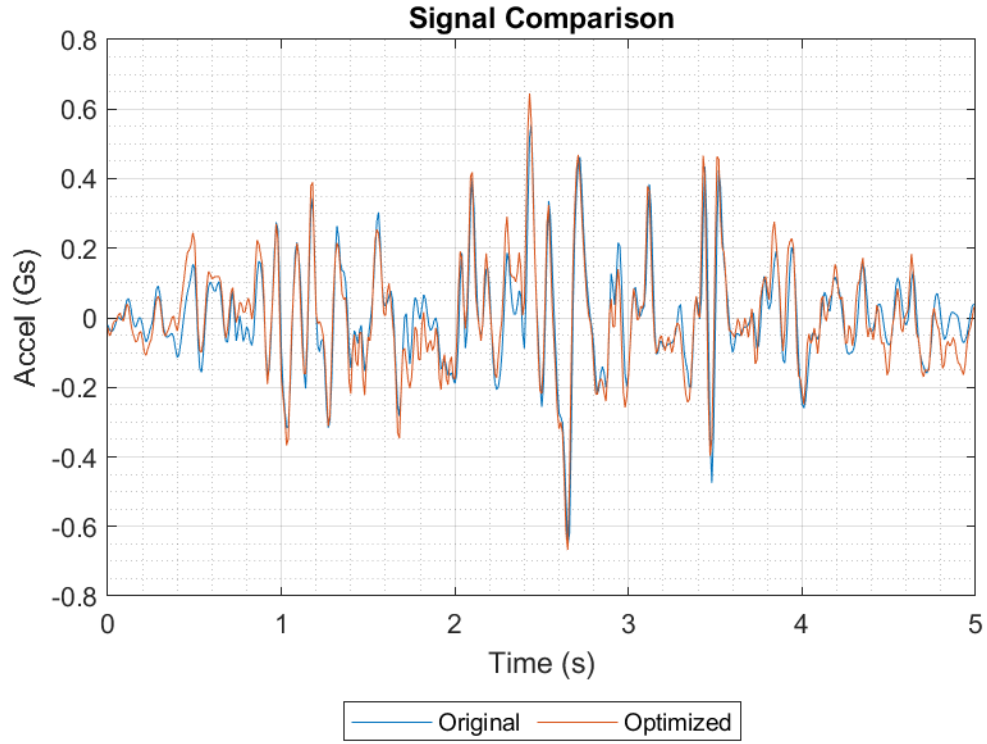


Figure 11. Comparison of Original and Optimized Signals in the Vertical Direction for an AFE of 1E-5

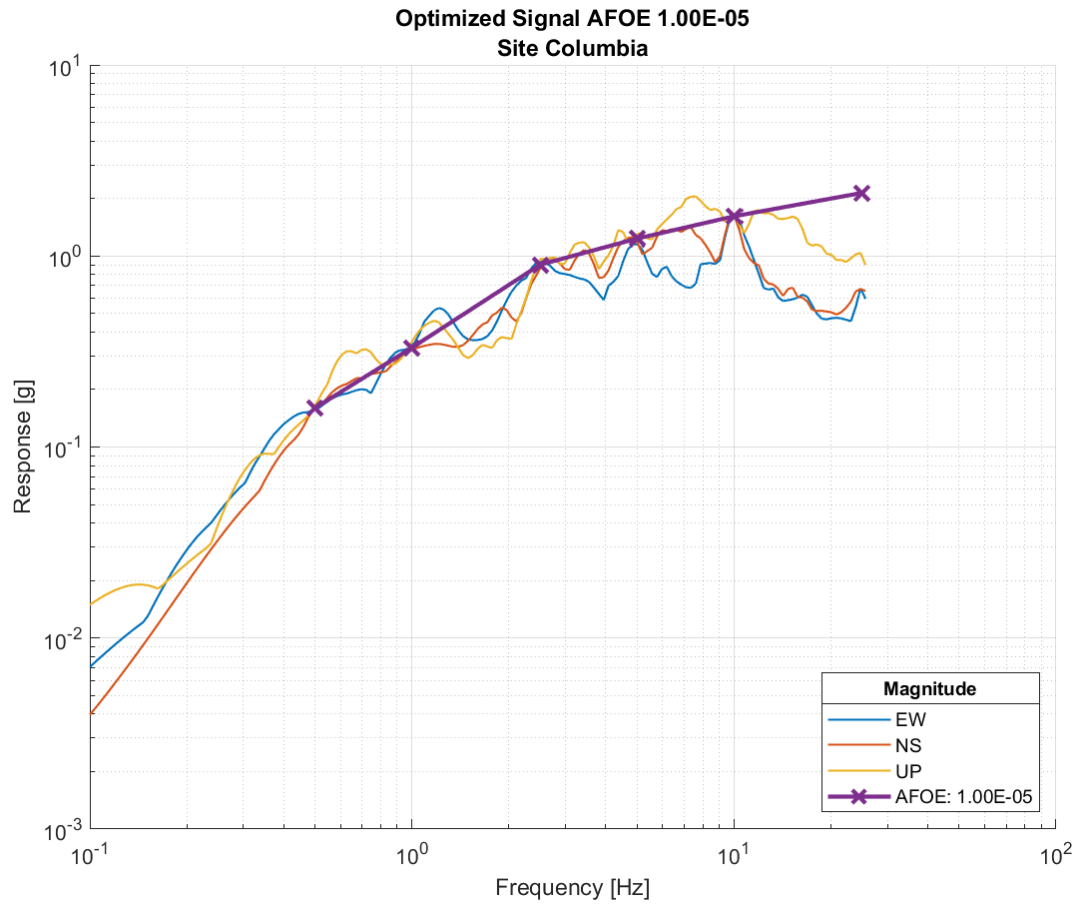


Figure 12. SRS of Optimized Signals for an AFE of 1E-5

## 5. CASK FINITE ELEMENT MODELING IN LS-DYNA

Cask system finite element modeling was conducted this year to start estimating the response range of the casks, canisters, and fuel assemblies in the planned test conditions. The test will take place on a shake table that can support and excite a full-scale, fully loaded cask system. Some significant preliminary modeling work was needed to help develop effective models of the cask system. An initial starting assumption was that explicit finite element methods are needed to accurately represent the nonlinear behavior of the full cask system when it is not anchored to a concrete ISFSI pad. Examples in the literature show explicit finite element modeling of SNF cask seismic response is common (NRC 2005), although the level of detail needed to include fuel assemblies within the cask would make it a very challenging problem because of the model size, complexity, and relatively long time duration (5 to 20 seconds) of earthquake loading. The LS-DYNA software has been used extensively by PNNL for structural dynamic analysis of SNF during transportation and cask drop scenarios. The seismic SNF cask modeling is an extension of the existing models and methods.

Preliminary models of the horizontal and vertical cask systems have been developed. These models do not yet represent the systems as they will be tested, but they are close. For example, the vertical cask system model has a lid on the top of the cask, and the SNF canister in both cases has a welded lid represented in the model. In the real test configuration, the lids are expected to be absent so cameras can view the motion of the fuel assemblies inside the canister. The mass and structural dynamic effects of the lids are expected to be minor, but noticeable, in the full system response. The next step in model development is to prepare pre-test prediction configurations, but at this time we do not yet have the correct shake table motions, which are due from SC Solutions later in the year.

The next sections describe the vertical cask system, horizontal cask system, and provide a summary of the modeling results to date.

### 5.1 Vertical Cask System Model

The vertical cask system will use the same NUHOMS® canister as that used in the horizontal cask system. The plan is to manufacture a mockup vertical concrete cask system to use in the test, as discussed in Section 3. The current vertical cask system model shown in Figure 13 is a defeatured representation of the vertical cask system shown in Figure 5.

The concrete pad modeled in the preliminary analyses and shown in Figure 13 is an elastic body that is 2 feet thick. During the test a layer of concrete is expected to be poured onto the shake table, so the coefficient of friction between the bottom of the cask and the shake table surface is representative of a real cask on a concrete ISFSI pad. No soil column underneath the pad, a typical feature in cask seismic models (for example, NRC 2005), is included in this model, but this representation more closely resembles the anticipated shake test conditions. Limited soil column modeling was explored this year and will be more fully discussed in a future report. All model results discussed in this report were generated from the elastic 2-foot pad model. Seismic excitation was applied to the pad as nodal prescribed motion on the sides and bottom of the concrete pad.

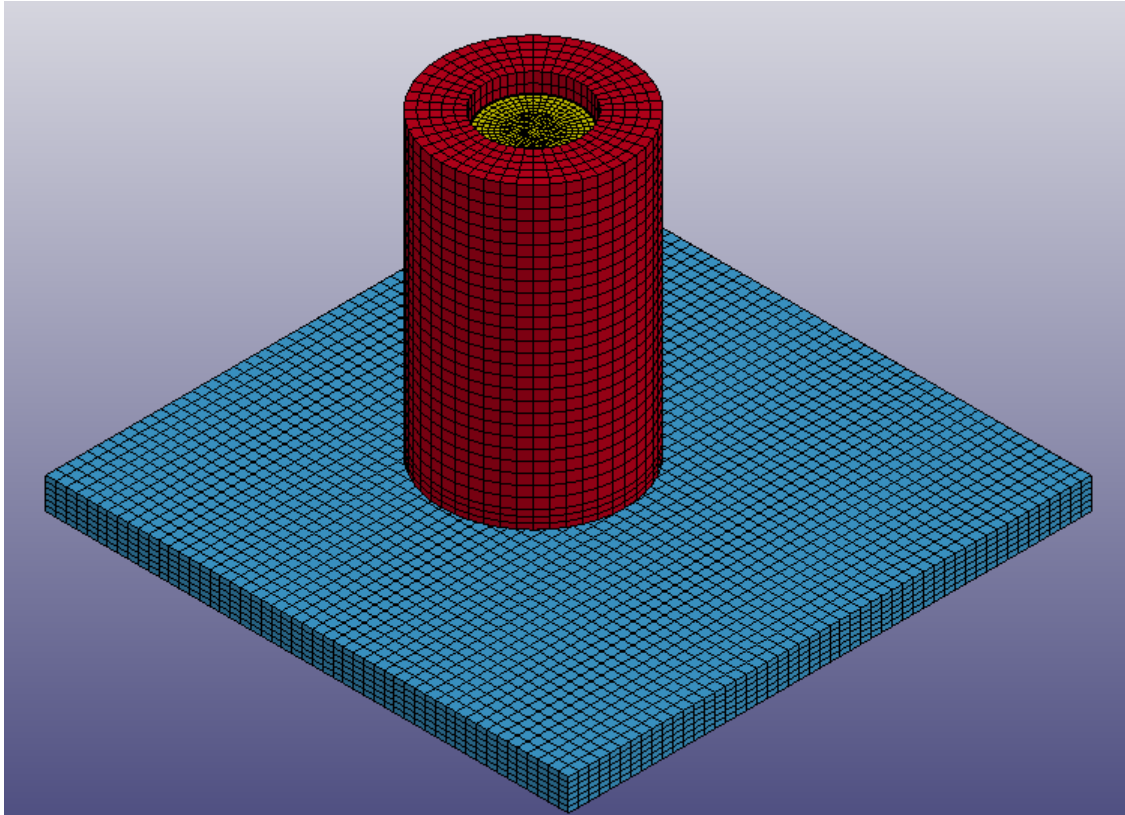


**Figure 13. Vertical Cask Model**

A cross section of the vertical cask model is shown in Figure 14. It is a relatively simple homogeneous concrete cylinder with a round hole to accommodate the canister. There is approximately 20 mm of radial gap between the canister and concrete cask wall when it is centered. The impact between the canister and cask is an important nonlinear driver of mechanical loads of the fuel inside the canister.

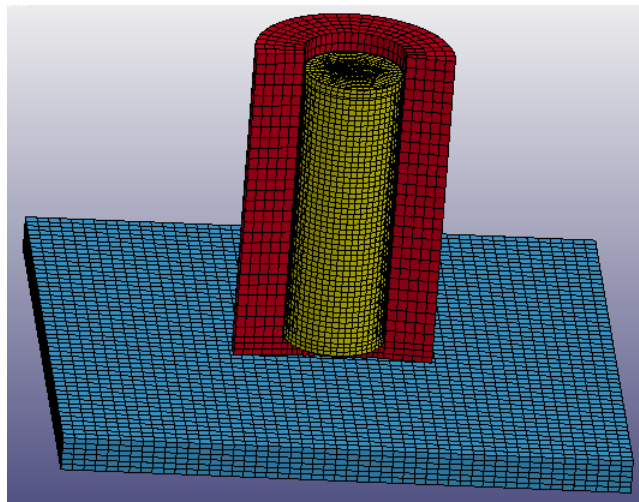


**Figure 14. Vertical Cask Model with Canister**

The canister model and its contents are shown in Figure 15. The canister has the same dimensions as the NUHOMS<sup>®</sup> 32P canister that will be used in the test. The grapple ring is not modeled and is not expected to have any significant effect on the structural dynamic response of the system. The basket is modeled as

a rigid shell structure whose primary purpose is to transfer contact forces between the canister wall and the dummy assemblies. The results show that the dummy assembly response varies throughout the canister because of the local opening and closing of gaps. The dummy assemblies are elastic bodies of approximately the same mass and outer dimensions as a real 16x16 PWR fuel assembly. As discussed in Section 3, the dummy assembly design is still being finalized, but the current dummy assembly model is expected to be a reasonable approximation of the fuel assemblies that will be used in the test.

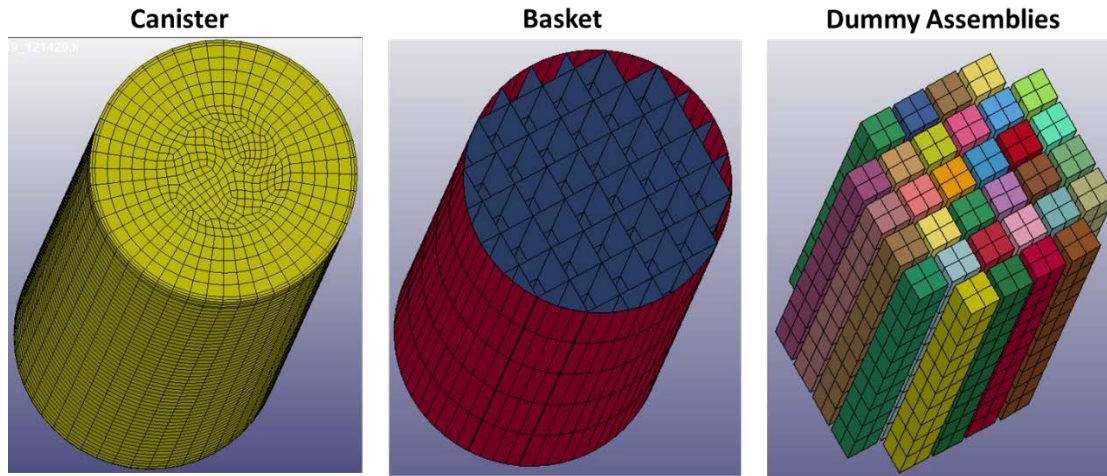


Figure 15. Canister and Contents Mesh

## 5.2 Horizontal Cask System Model

The horizontal cask system model represents the NUHOMS<sup>®</sup> Advanced Horizontal Storage Module – High Seismic (AHSM-HS). As planned, the test will use a real, as-manufactured NUHOMS<sup>®</sup> AHSM-HS unit with a 32 fuel assembly-capacity canister that was specifically designed to be used in the unit. The NUHOMS<sup>®</sup> system is designed to be connected to adjacent units in a long row configuration, but only a single unit will be used in the test. Initial modeling results indicate there is not a stability problem for testing a single unit, but this will be considered again when the proposed shake table time histories are provided by SC Solutions. Most of the analysis results of this report are derived from the vertical cask system because of concern about a vertical cask tip-over that does not apply to a horizontal cask system.

### 5.2.1 Model Geometry

The geometry for this seismic model is from the NUHOMS<sup>®</sup> AHSM-HS. Unlike the vertical cask system, this horizontal cask model was developed from the engineering drawings of the cask system that will be used in the test. Figure 16 shows a detailed solid model that is the basis of the finite element model. One important feature of this cask system is that it is designed to be deployed in a row of connected units, but we intend to use just a single unit in the shake table test. The solid model geometry can also be used to design a bracing structure if that is needed. The analysis described in Section 7.2 concludes that bracing is not needed for the preliminary seismic excitation that is considered in this report. The potential for the horizontal cask to tip over will be evaluated again when the proposed shake table motion is available.

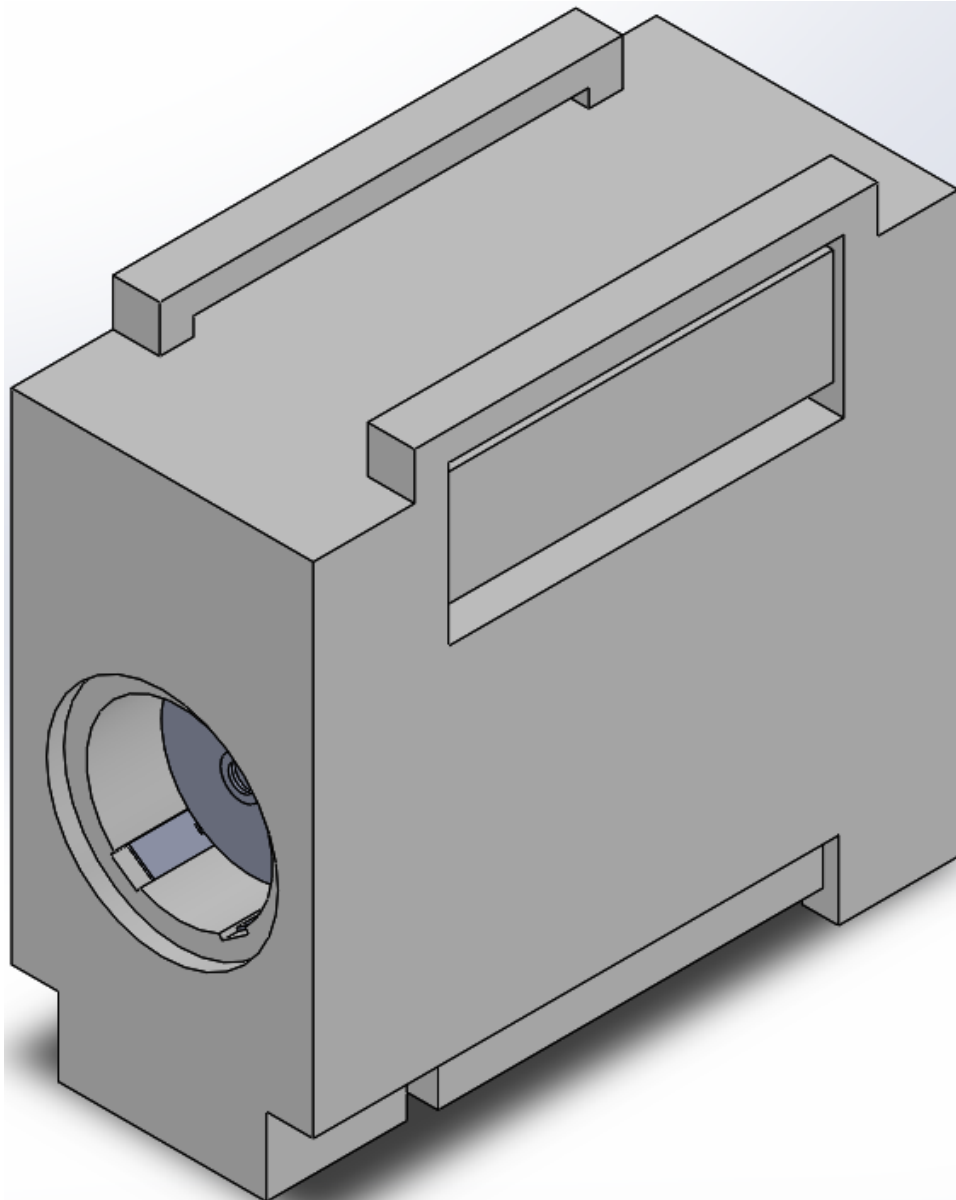


**Figure 16. NUHOMS® AHSM-HS Used for the Seismic Model**

### **5.2.2 ANSYS APDL to LS-DYNA**

The geometry was created and meshed with ANSYS APDL (Ansys Parametric Design Language) using a text input script. ANSYS was used to build the model because APDL is a very useful tool that allows for scripted model construction that makes it easy to modify the model as necessary to meet the needs of the analysis or to refine or optimize the model for computational efficiency. The ANSYS model was exported into LS-DYNA format, where final modifications were made. Figure 17 shows the model geometry as it appears in ANSYS.

To maintain a conformal mesh, the cask system was built as four separate components: cask overpack, canister support, canister, and concrete pad. Figure 18 shows the canister and the canister support components of the model. Figure 19 shows the model components with cut planes. These parts are connected using contact definitions in LS-DYNA. Figure 20 shows the complete horizontal cask finite element model.

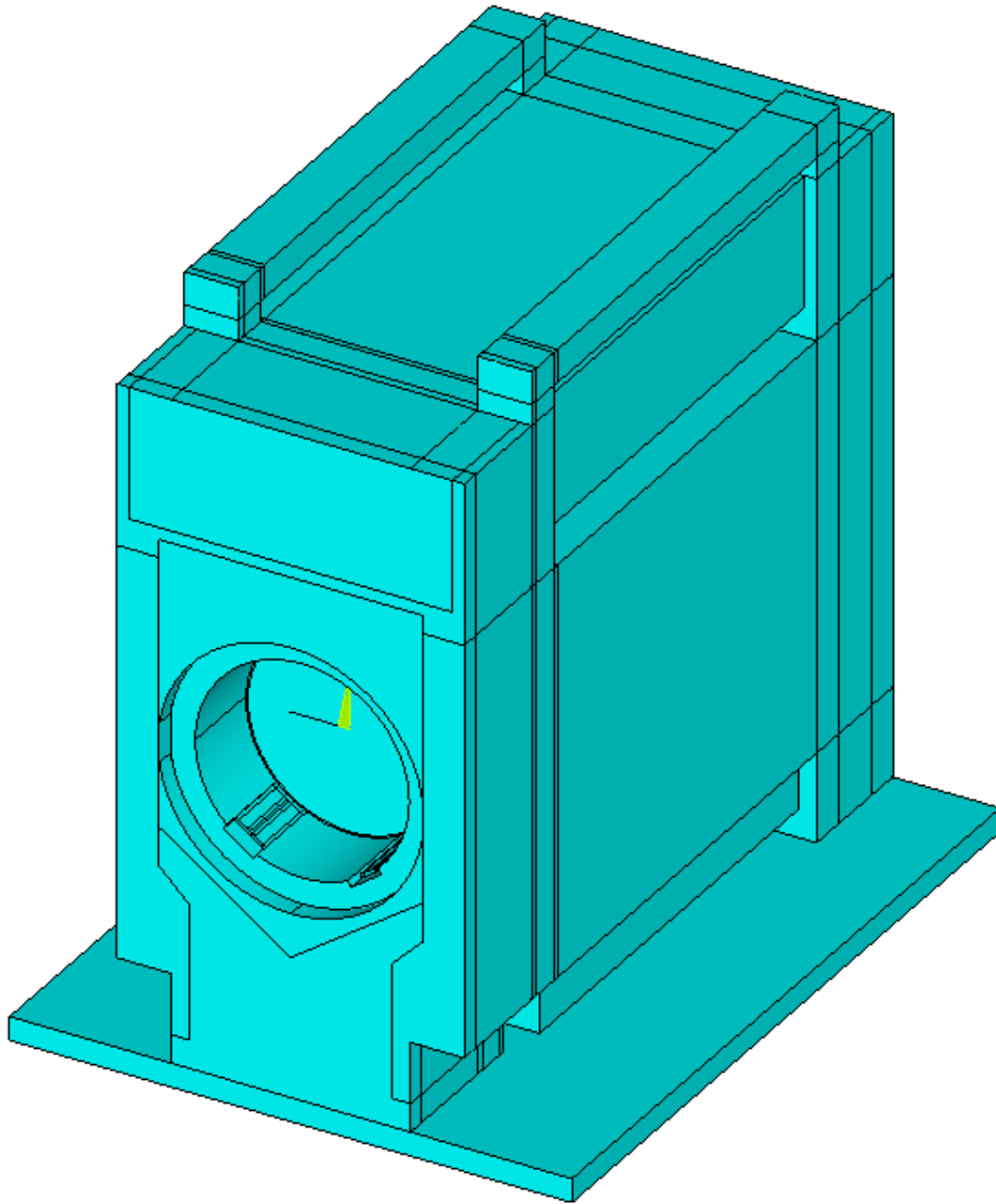


**Figure 17. ANSYS APDL Volume Plot of the Cask System Model**

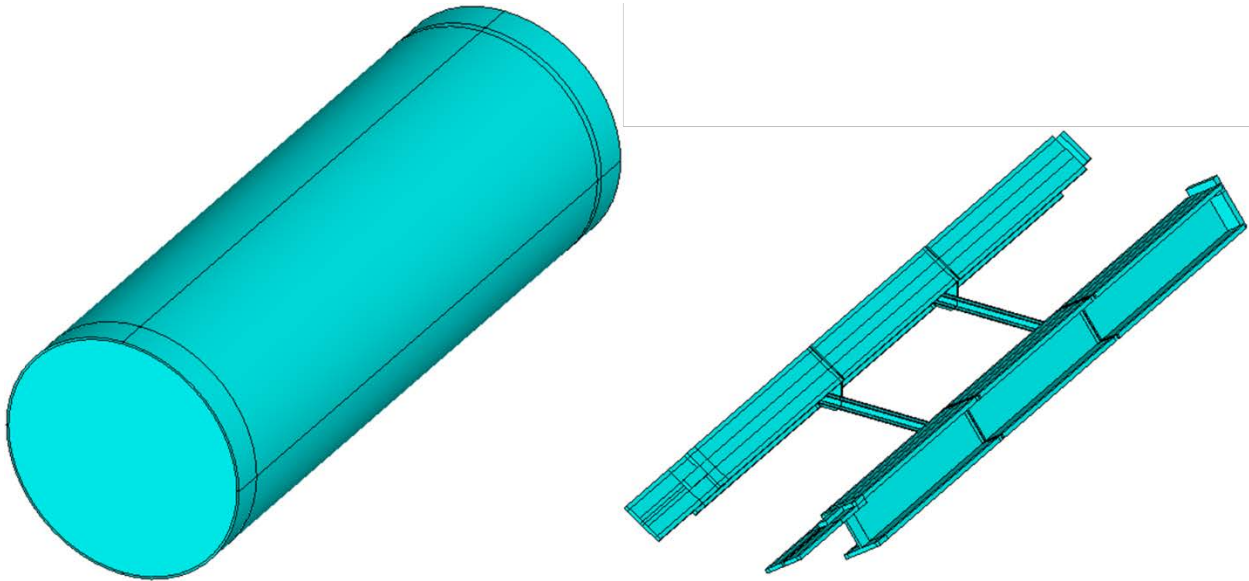


Figure 18. Canister and Support Structure Volumes from ANSYS APLD

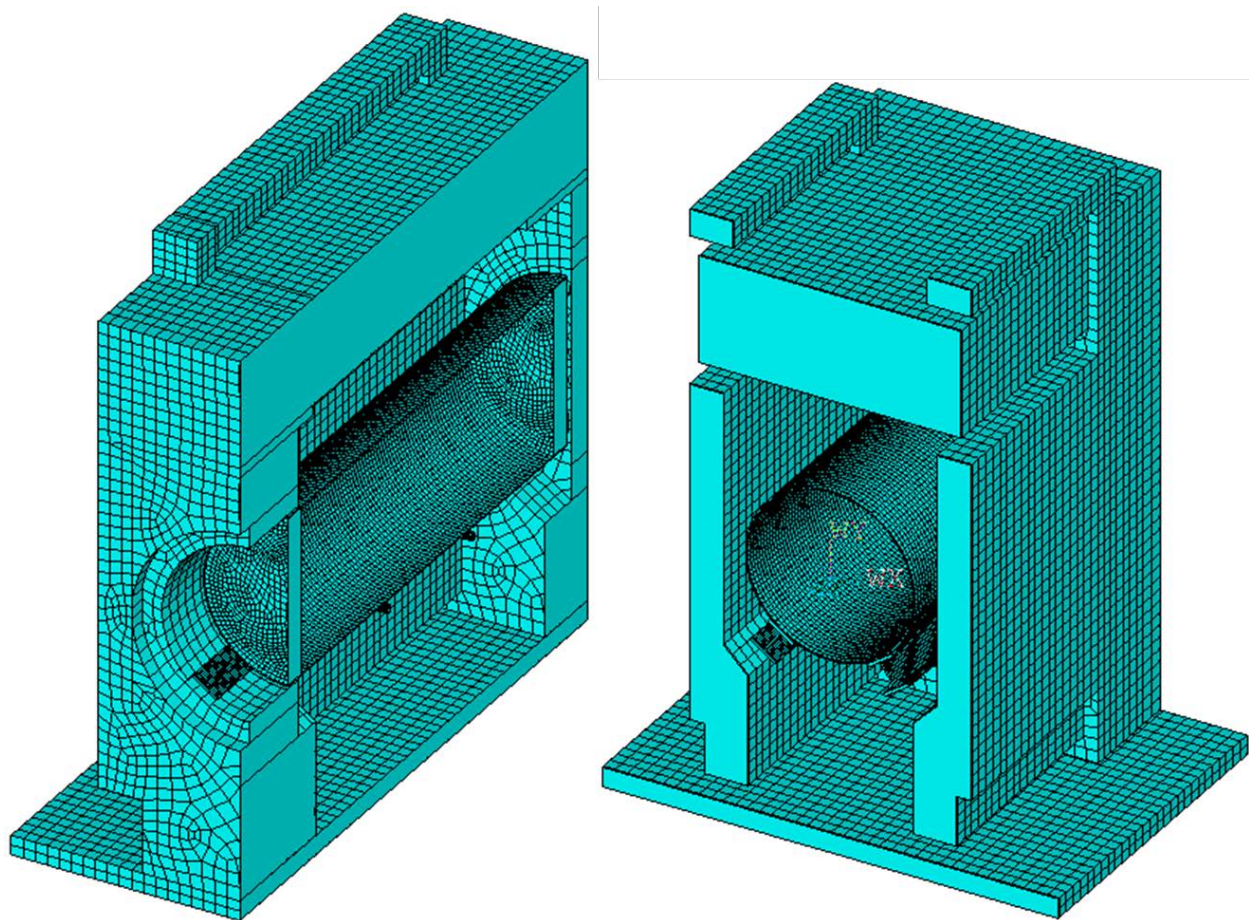
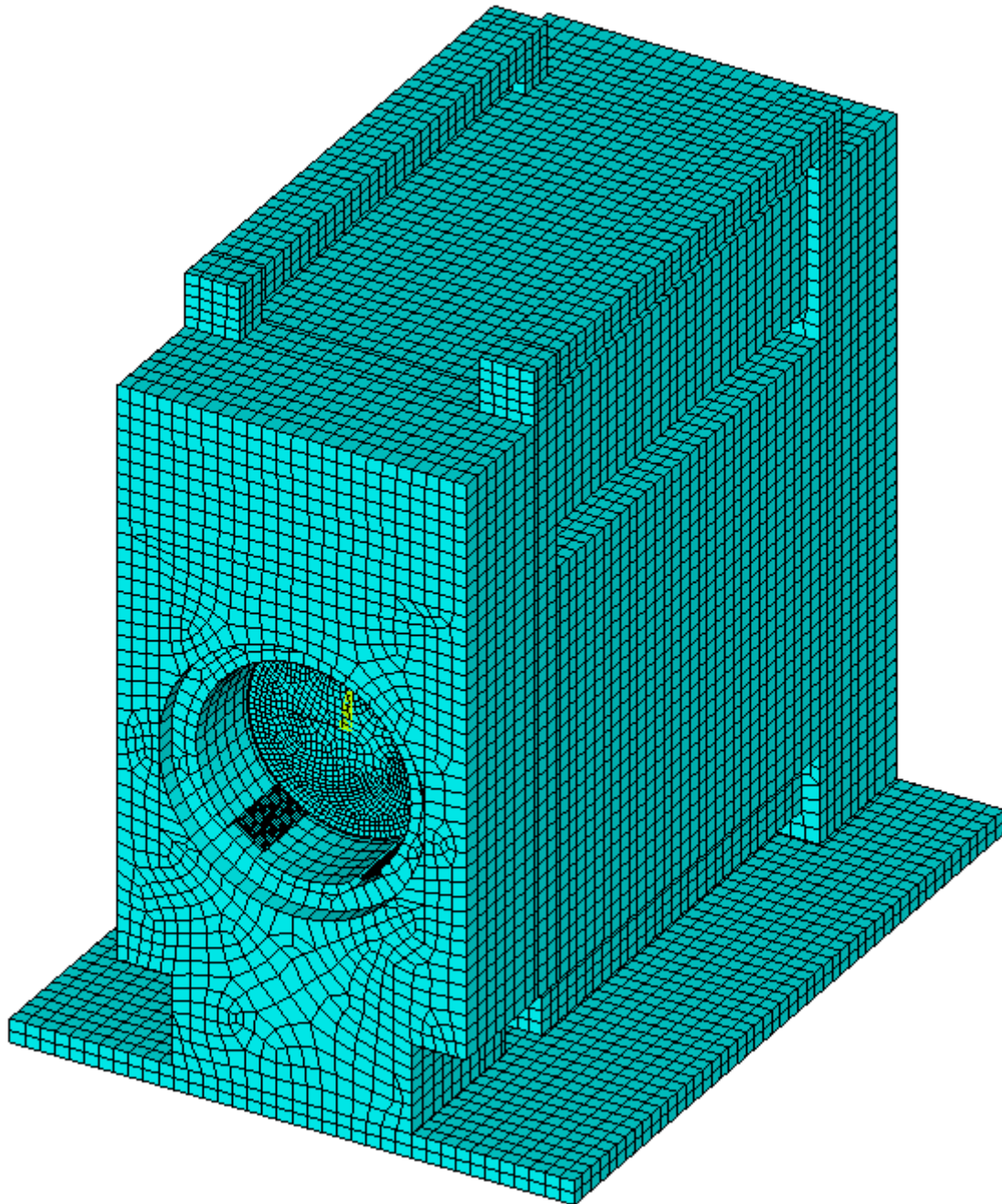


Figure 19. Element Mesh of the Cask Overpack, Canister Support, and Canister



**Figure 20. Exterior ANSYS APDL Element Plot**

The horizontal model is shown as it was evaluated in preliminary analyses in Figure 21. The pad was standardized to match the 2-foot-thick concrete pad developed for the vertical cask model (as described in the previous section). The finite element models in ANSYS (Figure 20) and LS-DYNA (Figure 21) are identical, with the differences in colors and appearance being the display settings of the two different finite element programs.

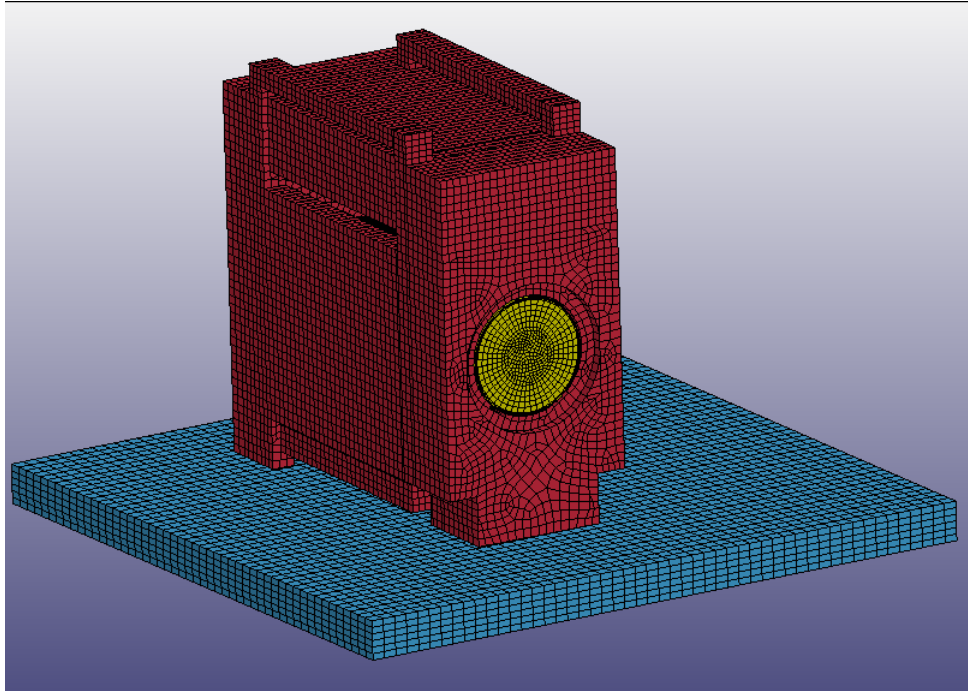


Figure 21. Horizontal Cask Model

### 5.3 LS-DYNA Modeling Results Summary

The cask system modeling is still a work in progress, but some interesting model results have been calculated. This section discusses a few key results that provide some relevant insight for the test.

Cask motion relative to the concrete pad is significantly influenced by the friction coefficients used in the model. Figure 22 shows the X direction displacement of the cask and pad in a case with low friction. The X direction is the stronger of the two horizontal motions, the Y direction is the weaker of the two horizontal motions, and the Z direction is vertical. The figure shows that the cask and pad strongly diverge in their motion before 3 seconds into the hypothetical earthquake. The friction coefficient in this low case is approximately 0.01 for the static and sliding components of friction. When the friction coefficient is set to 0.5, approximately no relative sliding occurs. Cask to pad friction is reported to have a significant variation of values in the technical literature—ranging from 0.2 to 0.8, as reported in NUREG/CR-6865 (NRC 2005). We used friction values of 0.01 to minimize friction forces to see their effect on the results. When pre-test predictions are prepared, they will consider friction in the 0.2 to 0.8 range.

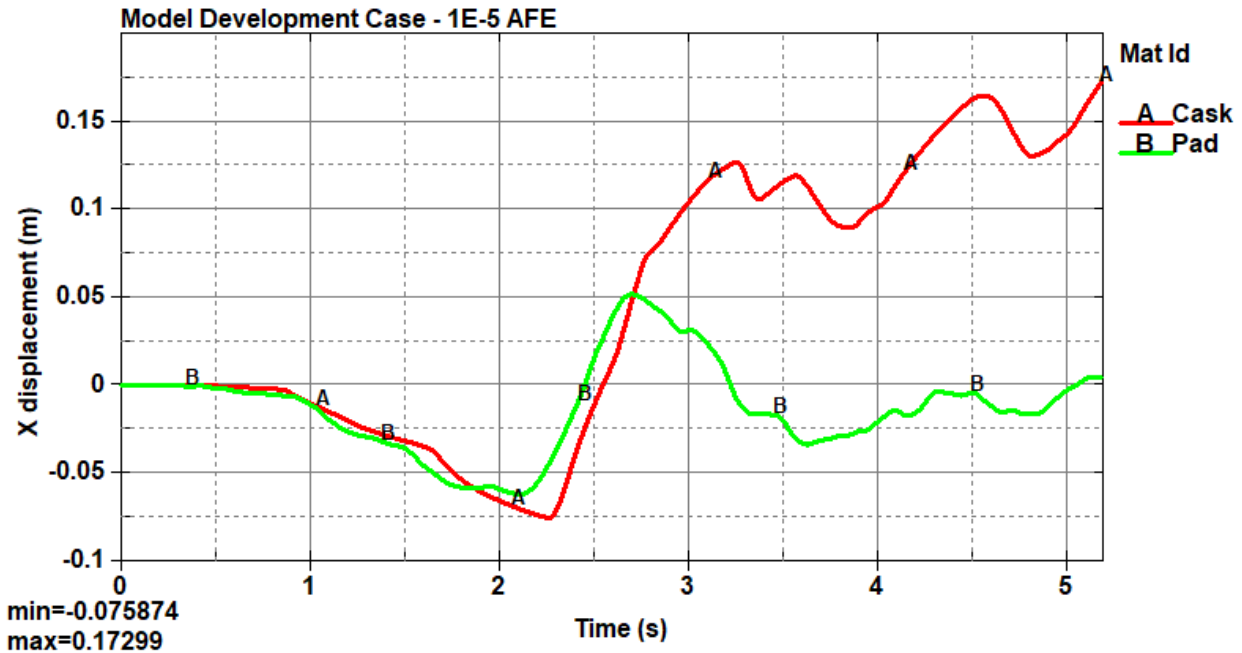


Figure 22. Low Friction Case

The cask and canister are predicted to have a significant amount of interaction. Figure 23 shows the X direction velocity of the cask and canister center of mass. Changes in velocity indicate accelerations. All of the canister accelerations are caused by forces transmitted to it from the cask. When the sign of the velocity value changes, it means the motion is changing direction. Changes in velocity are also changes in momentum—it takes significant forces applied over time to reverse a massive body’s momentum. However, the velocities of the cask and canister remain below 0.4 m/s, which is 0.9 miles per hour—slower than a slow walk.

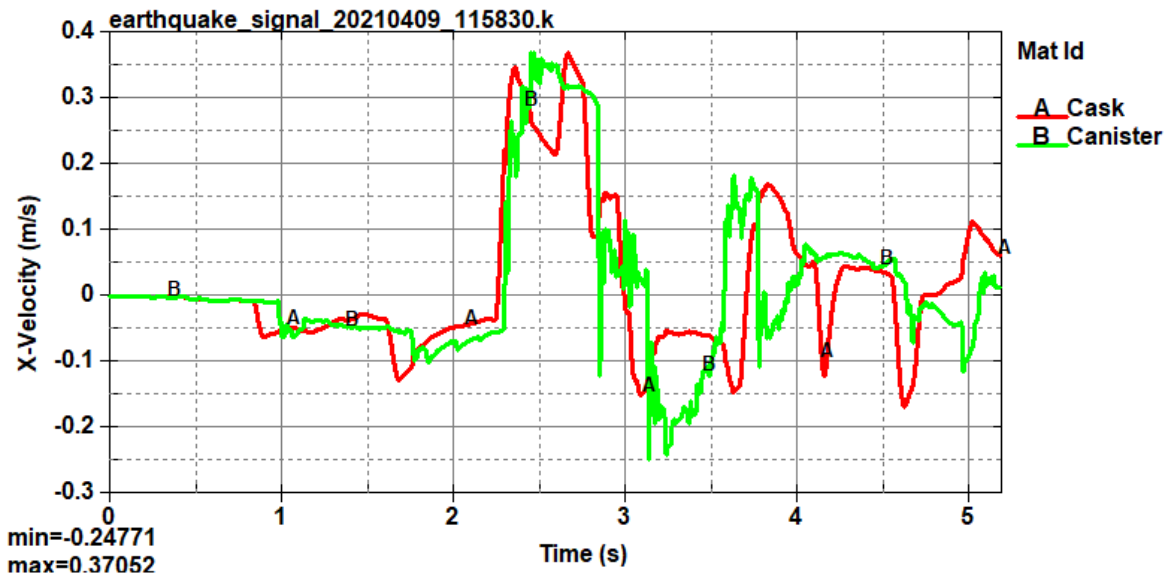
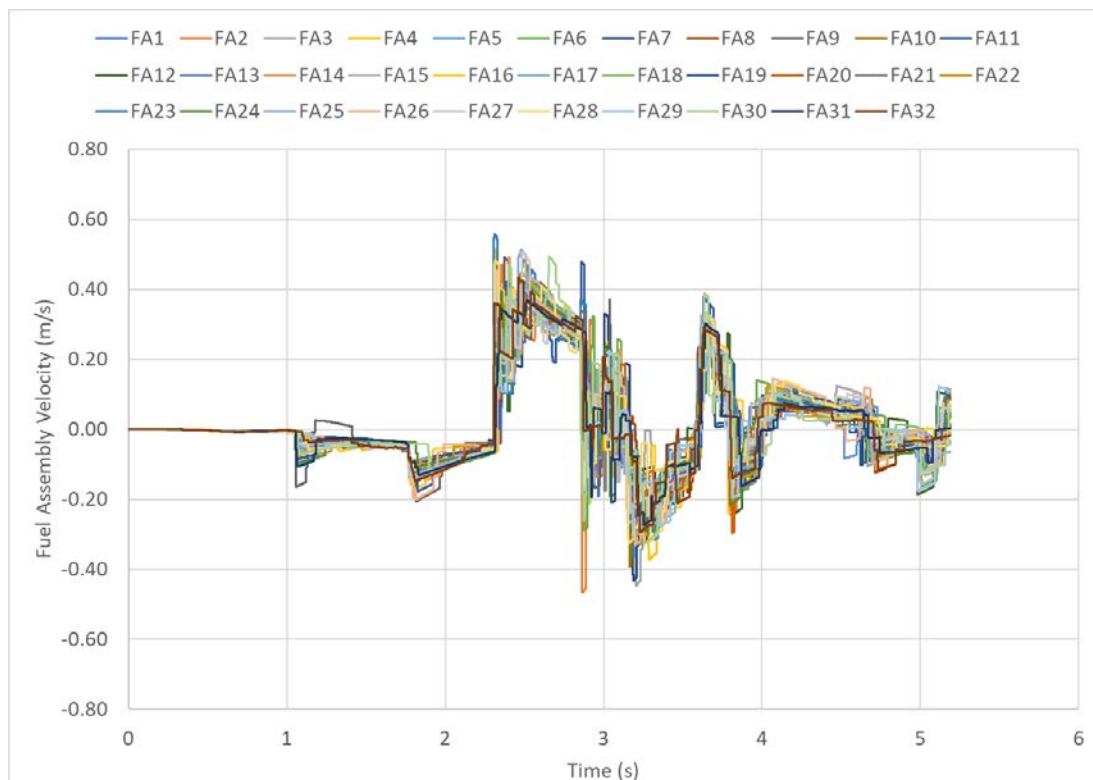


Figure 23. Cask and Canister Velocity in a Low Friction Case

The fuel assemblies inside the canister are predicted to experience faster velocities and stronger accelerations. Figure 24 shows the X direction velocity for all 32 fuel assemblies in the model. Changes in velocity indicate accelerations, and for fuel assemblies that typically indicates contact with the basket. The fuel assemblies reach higher velocities than the cask or canister (up to almost 0.6 m/s) but what is more distinctive is that each fuel assembly experiences a slightly different dynamic response. While all of the fuel assemblies broadly follow the same velocity trend, the variation in individual fuel assembly response suggests that the seismic response of fuel assemblies throughout the basket will be different. In the Multi-Modal Transportation Test (Klymyshyn et al. 2018), the basket location did not matter because the loads were so small. In the 30 cm cask drop test (Klymyshyn et al. 2020a), we witnessed a natural variation in the impact response due to variations in the gap distance prior to impact. The results shown in Figure 24 suggest that the dynamic response of fuel assemblies to the seismic loading case will be similar to the 30 cm cask drop response in its variation throughout the canister.



**Figure 24. Fuel Assembly Velocity in a Low Friction Case**

While a variation in fuel assembly response in the basket is expected, the higher friction case (0.5 static and dynamic friction coefficients) shows that higher friction could help cause a relatively more uniform response in the fuel. Figure 25 shows that fuel assembly response variation is still present in the 0.5 friction case, but compared to Figure 24 the spread of the curves is much narrower. These early model results suggest that friction could be a very significant phenomenon that needs to be well understood in order to predict the outcome of cask seismic events.

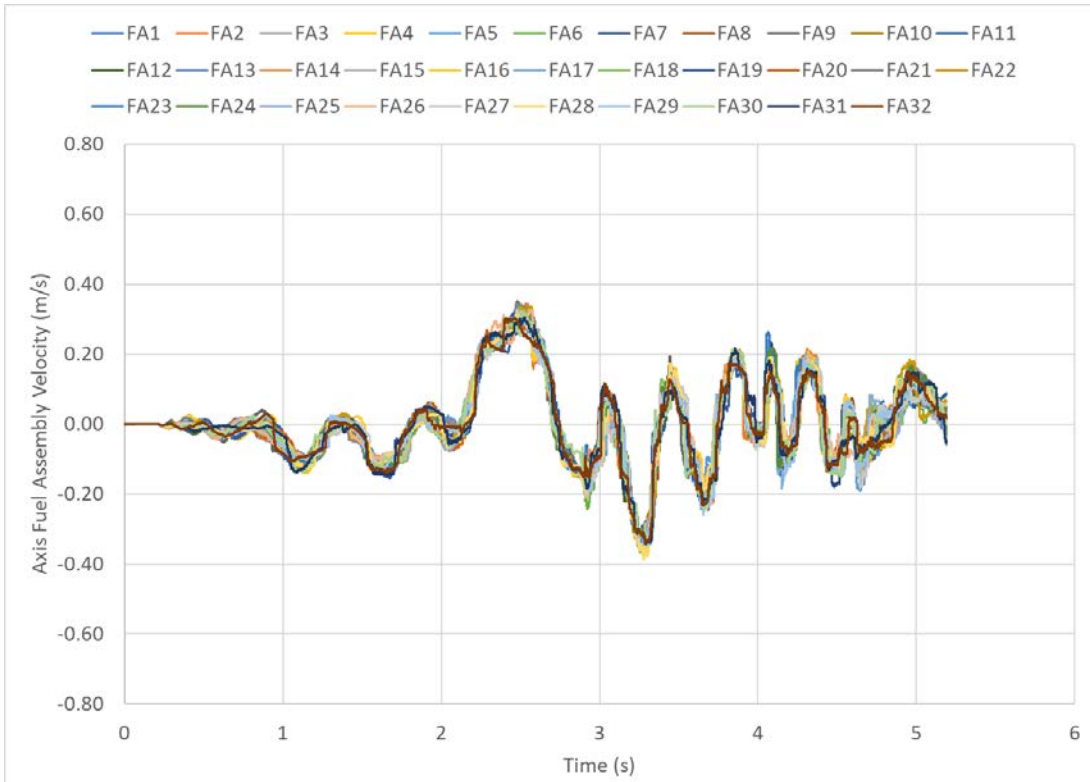


**Figure 25. Fuel Assembly Velocity in a 0.5 Friction Case**

This page is intentionally left blank.

## 6. FUEL ASSEMBLY MODELING

This section describes the first effort to predict fuel assembly seismic response from the cask system model. The methods are similar to previous PNNL modeling work that relates cask motion in transportation and cask drop scenarios to fuel assembly structural dynamic loading conditions.

### 6.1 Model Description

A finite element model was developed using LS-DYNA to simulate the response of a fuel assembly in a vertical storage cask to seismic excitation. The fuel assembly model is shown in Figure 26. The model represents a 17x17 PWR fuel assembly identical to the type used in previous modeling and testing campaigns including the Multi-Modal Transportation Test (MMTT) (Klymyshyn et al. 2018) and 30 cm drop scenario (Klymyshyn et al. 2020a). The fuel assembly is situated within a single basket cell, represented in the model as a rigid body. For additional information about the fuel assembly model, please refer to the fiscal year 2020 30 cm drop milestone report (Klymyshyn et al. 2020a). The model used here is nearly identical to the model used for the drop analyses, with the exception of the applied cask motion time history. Instead of being initialized with an initial velocity to simulate drop conditions, the model begins at rest and seismic excitation is applied to the basket. Excitation in three translational and three rotational axes is applied through the basket's center of gravity.

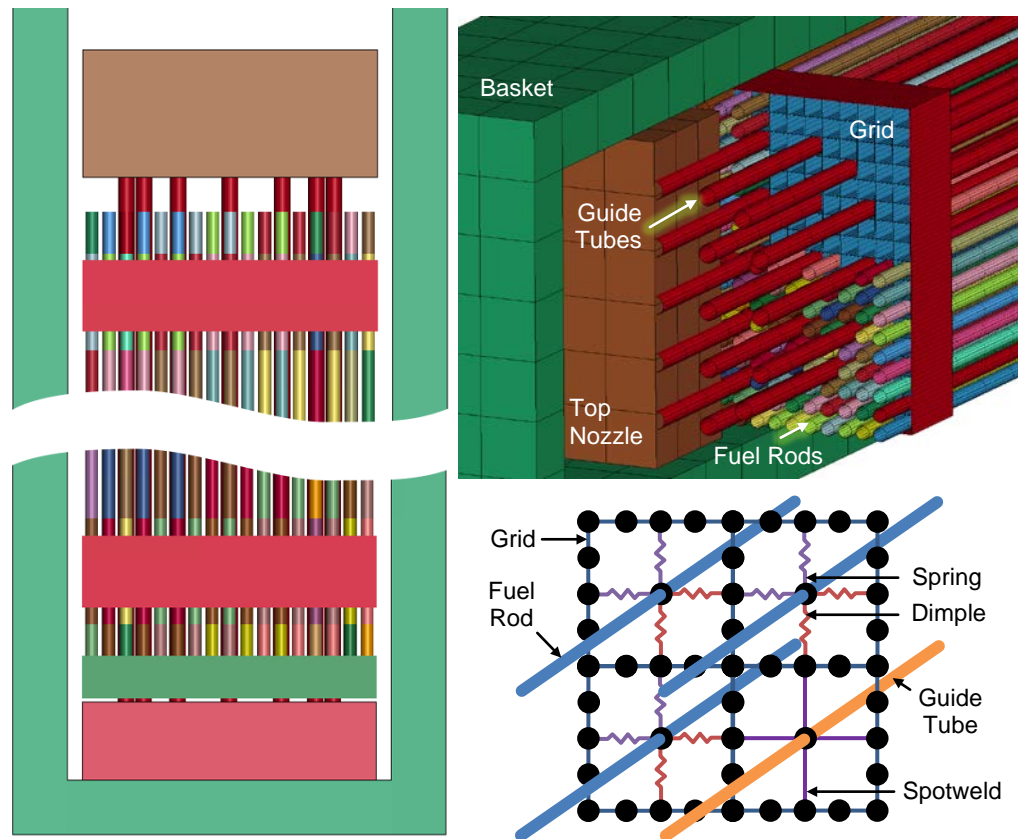
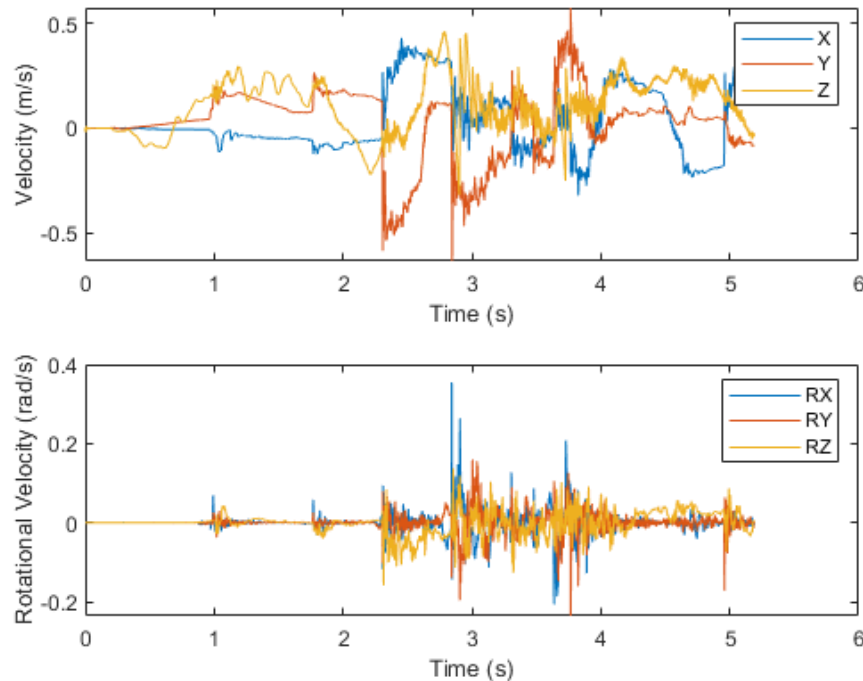


Figure 26. Fuel Assembly Seismic Model. Some parts have been hidden or sectioned for illustrative purposes.

## 6.2 Initial Modeling Study

The seismic excitation developed in Section 4 was used to excite the model in the initial modeling study discussed in Section 5.3. The applied time history is shown in Figure 27. Material properties were calculated at room temperature (22°C) and at low burnup (10 GWd).

The modeling results shown here represent a preliminary shakedown investigating the model performance and suitability for predicting the fuel assembly seismic response. Some aspects of the model are likely to be refined in the future, such as the excitation and fuel-to-basket gap size.



**Figure 27. Velocity Time History Applied in the Initial Modeling Study**

Overall fuel assembly dynamic behavior and fuel, guide tube, and spacer grid deformation responses are detailed in the subsequent sections.

### 6.2.1 Preliminary Results – Fuel Assembly Dynamics

The motions of the fuel assembly relative to the basket and impact between the fuel assembly and basket were observed as a result of the applied seismic excitation. Figure 28 shows the displacement of the bottom nozzle relative to the basket floor. The model is configured in its initial state with an 11 mm gap on each side of the fuel assembly, thus the lateral (X and Y) displacement is limited to the size of that gap. Virtually no sliding of the fuel assembly occurs until approximately  $t = 2.4$  s, but by approximately  $t = 3.9$  s, the seismic excitation is sufficient to cause complete gap closure (impact between the bottom nozzle and basket) on one side of the fuel assembly. This model assumed static and dynamic coefficients of friction equal to 0.25, which is relatively low for clean, dry metal-on-metal contact. Future modeling efforts should include a sensitivity study to investigate the effect of coefficient of friction on the SNF response.

Gap closure also occurs at the top nozzle and along the length of the fuel bundle, as illustrated in the plots of resultant X-Y acceleration in Figure 29. Large peaks in the top nozzle acceleration indicate multiple impacts between it and the basket. Multiple impacts between the fuel bundle and the basket were also observed. The peak nodal average acceleration on a representative fuel rod was up to approximately 14 g.

For comparison, this is smaller than the nodal average fuel rod acceleration in the horizontal 30 cm drop model, which ranged from 45–82 g (Klymyshyn et al. 2020a). On the other hand, it is larger than the fuel rod accelerations measured in the westbound rail segment of the MMTT, which were less than 1.5 g (Klymyshyn et al. 2018).

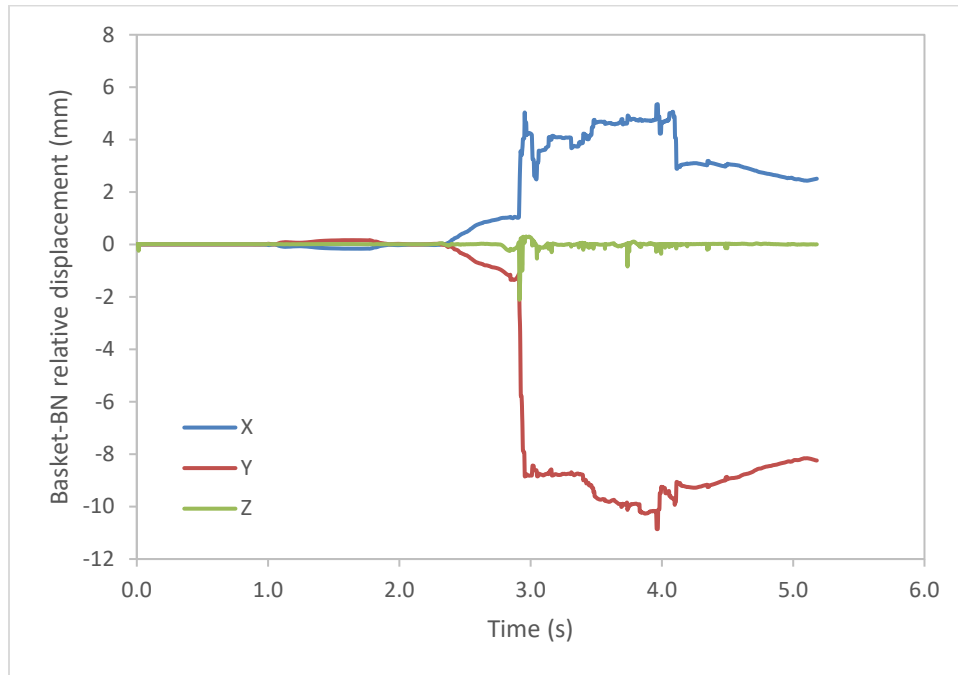


**Figure 28. Displacement of Bottom Nozzle Relative to Basket Floor**

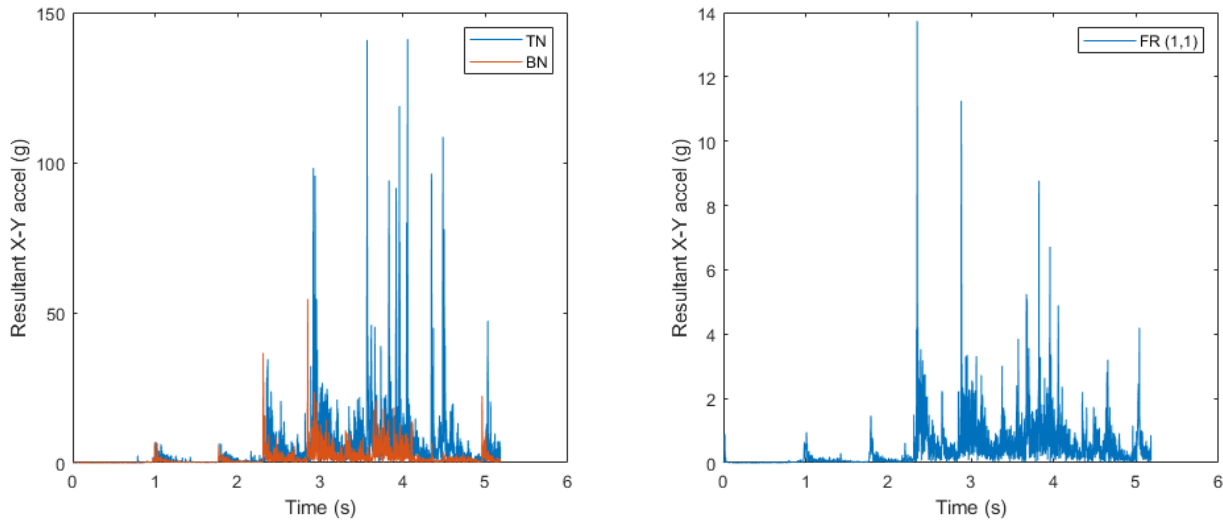


**Figure 29. Top and Bottom Nozzle (left) and Representative Fuel Rod (right) Resultant Acceleration**

## 6.2.2 Preliminary Results – Fuel Assembly Component Deformation

Fuel rod and guide tube strains are visualized with respect to magnitude, position, and time in Figure 30 through Figure 32. All of the strain data have been filtered with a sixth-order Butterworth low pass filter with a cutoff frequency of 300 Hz. This treatment is to remove numerical noise from the simulation and is equivalent to the filtering done for the 30 cm drop modeling campaign (Klymyshyn et al. 2020a)

The peak fuel rod cladding strain was about 1700  $\mu\text{E}$ , located in the lowest span of the fuel assembly. This strain is well below the yield strain of the cladding, which in this model is approximately 11,000  $\mu\text{E}$  at 22°C and 10 GWd/MTU burnup (Geelhood et al. 2018). This reflects lower order bending modes where the bottom of the assembly is stationary and the upper portion of the assembly moves freely. As shown in Figure 30 and Figure 31, the strain tends to be highest near the bottom of the assembly, with concentrations of strain near the grid spacers. Plastic strain of 1–2% was detected near the top of the guide tubes, but closer inspection of the model suggests that these are spurious strains due to a contact instability associated with the coarse mesh of the basket and top nozzle. Outside of this region, the guide tube strain is limited to approximately 2500  $\mu\text{E}$ , which is well below the yield strain, which in this model is approximately 7500  $\mu\text{E}$  at 22°C and 10 GWd/MTU (Geelhood et al. 2018). Figure 32 shows the evolution of the fuel rod and guide tube strains over time, with respect to elevation. This method of displaying the data is useful for showing which parts of the seismic excitation time history are most damaging to the fuel. The peak fuel rod cladding strain occurs at around  $t = 3.7\text{s}$ , but there are other periods in the time history that show similarly high strains such as at  $t = 2.3\text{s}$  and  $t = 3.0\text{s}$ .

The cladding strains observed in this preliminary study are similar to those observed in the 30 cm fuel assembly drop test, but much less than the strain predicted in generic modeling studies of the 30 cm drop scenario (up to 4700  $\mu\text{E}$  [Klymyshyn et al. 2020a]). Regardless, the cladding strains are well under the yield strain for Zircaloy and the fuel integrity does not appear to be challenged. The guide tube strains are of interest because of the plastic strain observed, but at this time these strains are not considered credible. Further investigation and model refinement are needed to determine the loads on the fuel assembly load chain.

Finally, Figure 33 shows the lateral deformation of selected spacer grids. Strains in the two uppermost and also the lowermost grids are plotted. The uppermost grids tend to see higher deformations due to the propensity for the upper regions of the fuel assembly to impact the basket, but these deformations are limited to small fractions of a millimeter. In contrast, visible grid buckling and crushing of 5–6 mm were observed in the SNL 30 cm drop test. Grid buckling and crushing do not appear to be major concerns for the fuel assembly seismic response.

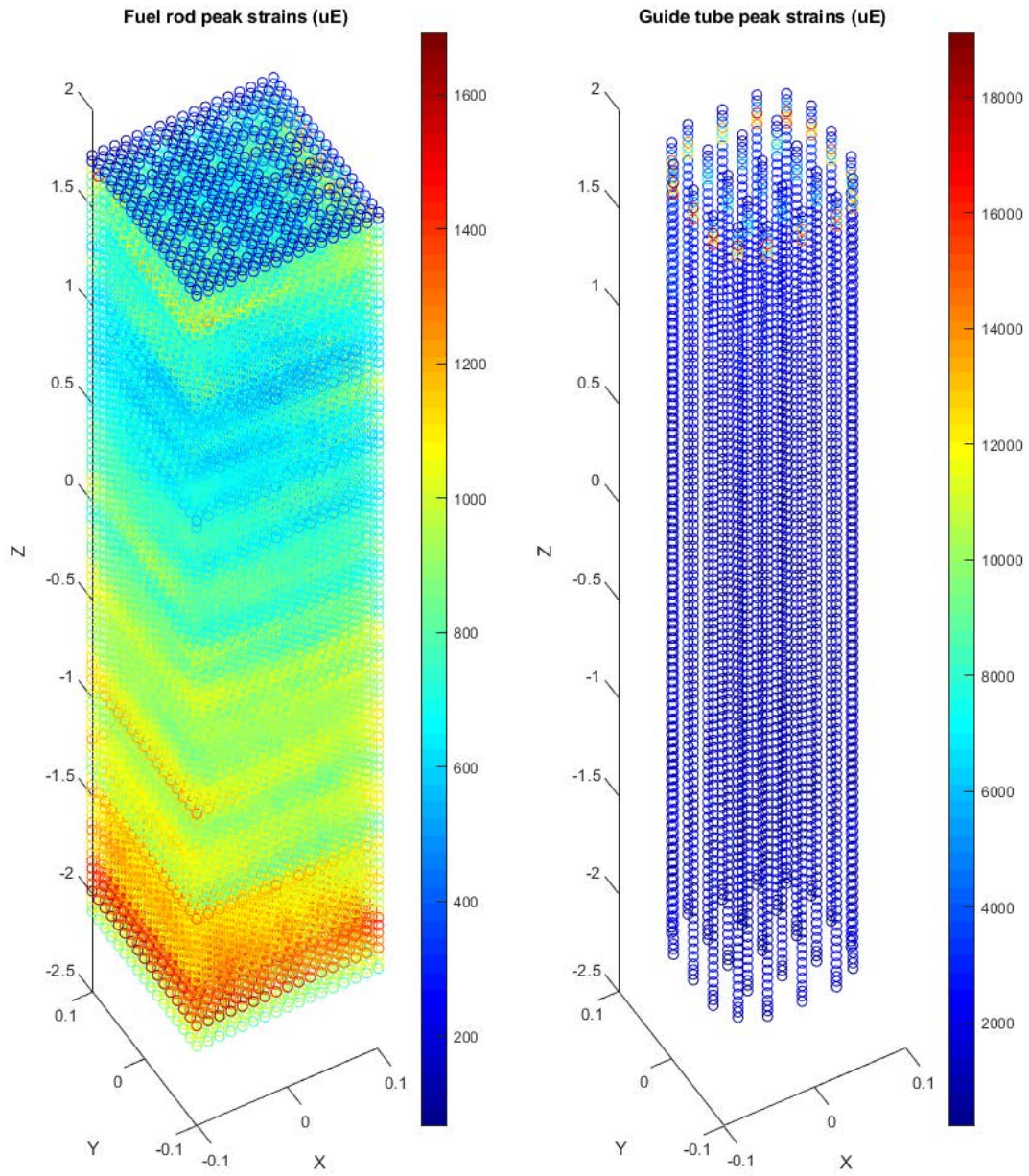
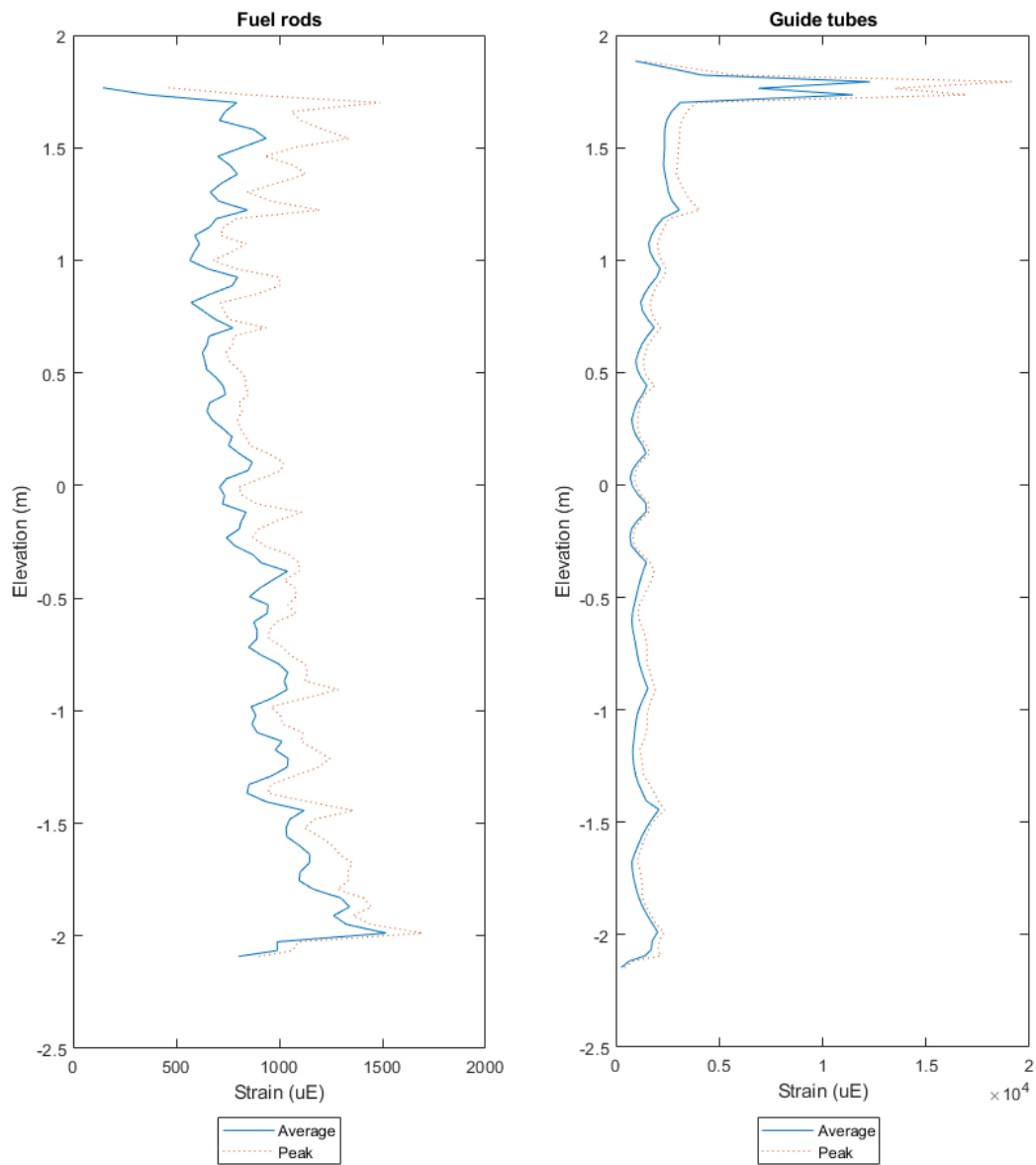


Figure 30. Fuel Rod and Guide Tube Peak Strains



**Figure 31. Peak and Average Fuel Rod and Guide Tube Strains as a Function of Elevation**

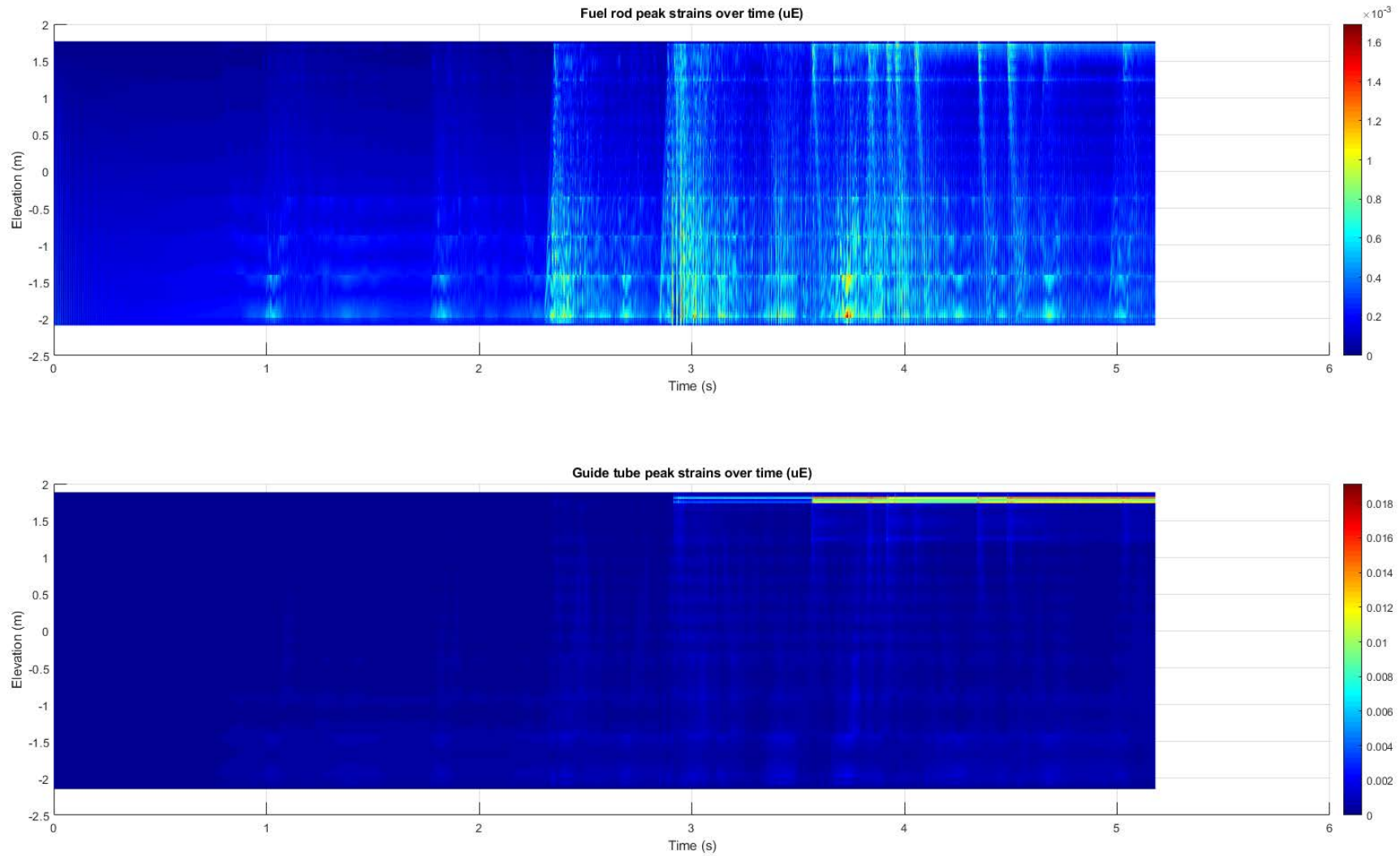
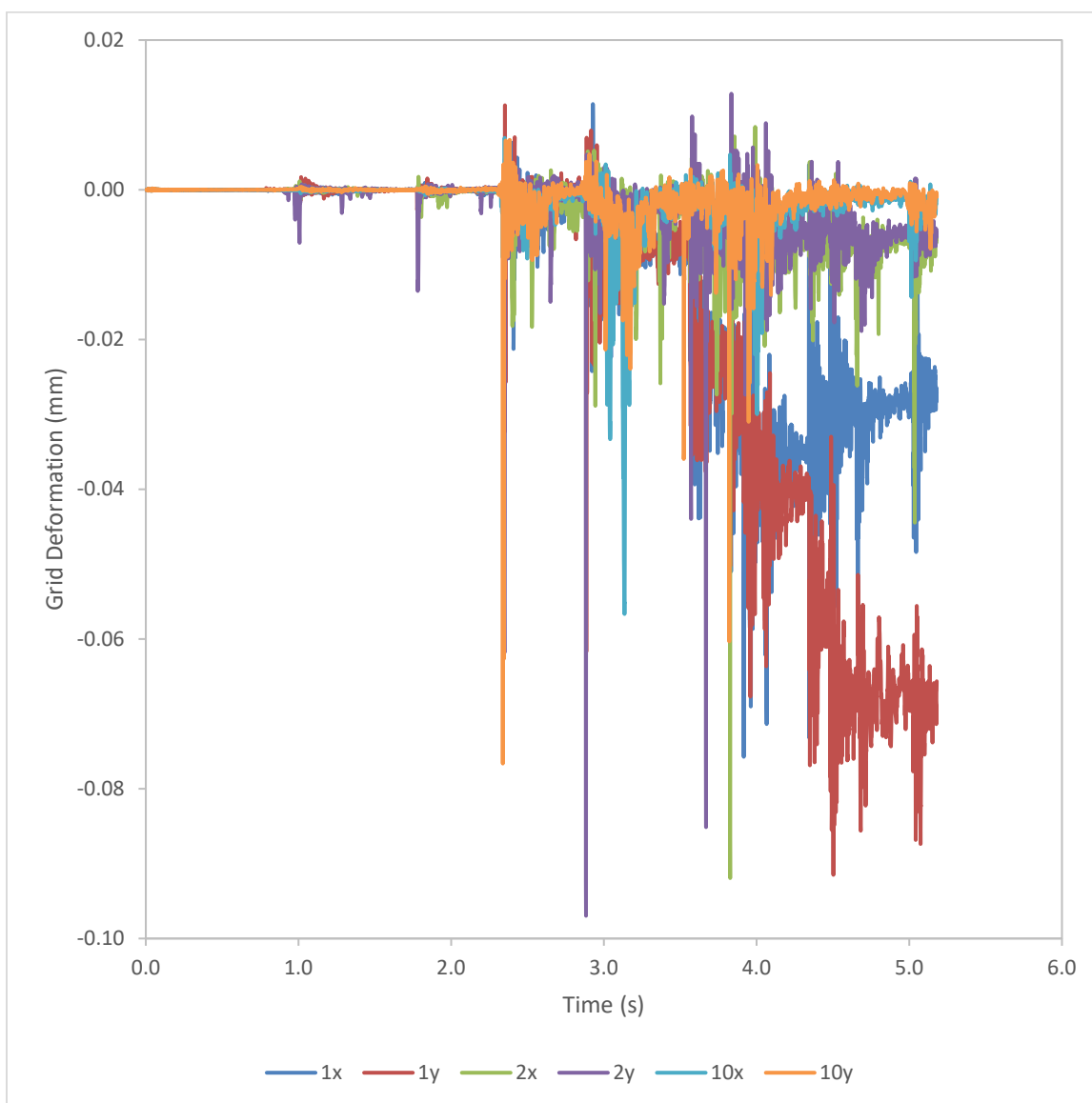


Figure 32. Peak Fuel Rod and Guide Tube Accelerations as a Function of Elevation and Time



**Figure 33. Grid Deformation in Both Lateral Directions (X and Y) in the Uppermost Grids (1 and 2) and Lowermost Grid (10)**

### 6.3 Outlook

A preliminary modeling study has been performed to evaluate a detailed fuel assembly model for use in modeling SNF response to seismic events. The results indicate that fuel strains remain well below yield, in line with previous testing and modeling of SNF under normal conditions of transport. These results are preliminary and additional model refinement and sensitivity studies are needed to gain further confidence in the model. Notable areas for further research are the use of a range of more realistic seismic excitation data and a range of fuel-to-basket gaps characteristic of actual in-service configurations. The response of different fuel types such as the 16x16 PWR assemblies to be used in the test campaign should also be investigated.

## 7. TEST CONSIDERATIONS

The purpose of the modeling at this stage is to help inform the test plan. Certain details and choices need to be evaluated to determine if they should be implemented in the test plan. For example, an early question came up about whether it would be appropriate to include instrumented 17x17 PWR surrogate fuel assemblies in the canister, when it was originally designed for 16x16 PWR assemblies. The mass and geometry of the two different PWR fuel assembly types are different, so it is reasonable to estimate the consequences of using mixed assembly types and dummy assemblies in the test. The considerations are summarized below, and ensuing sections will provide the details of the analysis when they are available.

- **Mixed Fuel Assemblies in Canister (7.1).** Analysis indicates that differences in fuel assembly geometry and mass will have some effect on the loads transmitted to the fuel assemblies in the basket, but the fuel assembly mechanical loads are not uniform, even when all fuel is identical. The gaps between fuel assemblies and the surrounding basket make fuel assembly response nonlinear. The response of the same canister contents to seismic excitation is expected to vary somewhat based on initial conditions (such as precisely where the fuel assemblies are located within their basket locations). It is impossible to place fuel assemblies in the center of the basket before each test, so some variation in the response of the test will occur. **Conclusion:** Mixing fuel assemblies and using dummy assemblies with variable gap sizes is an acceptable test detail.
- **Horizontal Cask Considerations to Avoid Tipover during Testing (7.2).** Horizontal casks are never deployed individually. When we test one, do we need to add a bracing structure to keep the cask from tipping over? Additionally, should we restrict testing to 2D motion (longitudinal and vertical, no lateral motion)? Analysis of the preliminary models indicates that the horizontal cask will not tip over in its unmodified state for the 3D working shake table motion described in Section 4. **Conclusion:** There is currently no tip-over concern for the horizontal cask, but this should be reassessed using the planned test configuration when we have the real shake table motion to use in the models.
- **Need for Open Canister Bracing.** The test plan is to run the seismic shake test using a canister that does not have a lid attached. Omitting the lid allows the instrumentation wires to be routed effectively and allows cameras to record the fuel assembly motion. However, the lid is a massive, structurally significant component, so its absence is expected to alter the dynamic response of the system. The amount of influence on the system response will be estimated by modeling. There may be a need to add a bracing structure to prevent the open end of the canister to flex (or deflect, or ovalize) during testing. This evaluation will be done when the pre-test prediction models are completed. **Conclusion:** The need for canister bracing has not been evaluated yet.

### 7.1 Mixed Fuel Assemblies in the Canister

The intent is to use 16x16 and 17x17 PWR surrogate assemblies to record the response of different fuel assembly configurations during the seismic test. As planned, the test also will use dummy assemblies that have a variable gap distance between the dummy assembly contact points and the fuel basket walls. The primary effect of these features is a nonuniform gap distribution throughout the canister. The preliminary models suggest that the presence of nonuniform fuel assemblies has an effect on the loads transmitted to the fuel assemblies over time, but it does not significantly change the range of loads or the extreme values.

The vertical cask model described in Section 5.1 was modified such that one dummy fuel assembly was reduced in height and width. The height of Fuel Assembly 1 (FA 1) was reduced to 90% of standard and the solid square cross section width was reduced to 95% of standard. The density remained as the

standard value, so the reduced size of FA 1 also contributed to a proportional reduction in mass. The reduction in width of FA 1 also changed its relative position in the basket cell, shifting it slightly off center. Figure 34 shows the X direction velocity trace of all 32 fuel assemblies in the normal balanced case (left) and the special unbalanced case (right) that has the reduced dimensions for FA 1. The applied motion to the pad is the same in both cases. It is observed that the change in FA 1 alters the velocity history of every fuel assembly in the canister. Another observation is that the unbalanced case has a similar positive peak and a lower negative peak, which suggests that the unbalanced case could be more limiting in terms of fuel assembly mechanical loads.

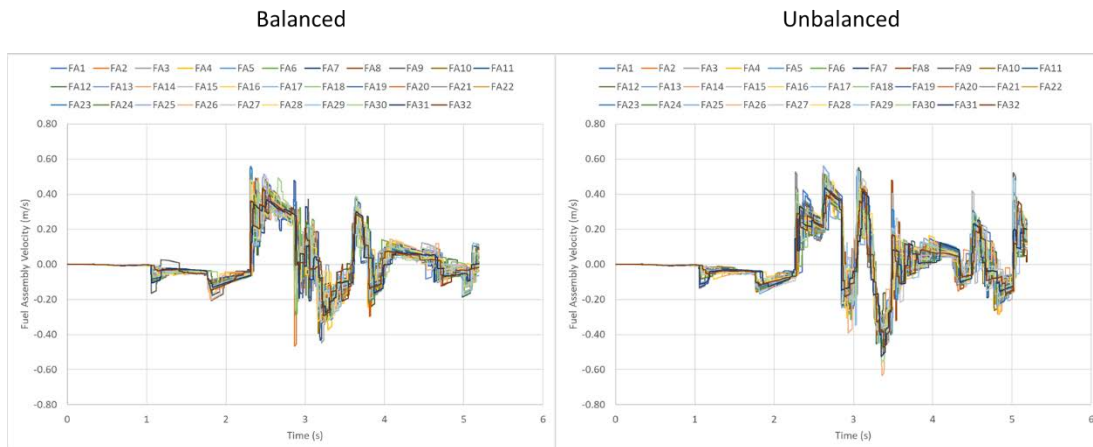


**Figure 34. Fuel Response in a Vertical Canister: Balanced (Left) and Unbalanced (right)**

A conclusion drawn from this study is that each individual fuel assembly can affect the seismic response of all fuel assemblies inside the canister. This suggests that the seismic loading environment is uncertain and difficult to predict or recreate. The variation in the response of fuel assemblies observed in all model cases is also important to note. It appears that, similar to the 30 cm cask drop testing (Klymyshyn et al. 2020a), we should not expect the loads applied to fuel assemblies in a canister to be equal even when the fuel assemblies are identical.

This test is a rare opportunity, so there is a desire to test a variety of different PWR fuel assembly designs to record their mechanical responses. Based on the model results, there is no reason to restrict the test to identical or closely similar fuel assemblies – even identical fuel assemblies are expected to have different loads throughout the canister.

A related observation is that the gap conditions between each fuel assembly is an important initial condition in the model and in the test. Section 5.3 discussed the variation of fuel assembly response, which is observable in Figure 34 (left). The balanced case had perfectly centered fuel assemblies as its initial condition. It is straightforward to define specific gap conditions to each fuel assembly in the model, but it is not practical to try to control the gap conditions in the test. It is recommended to perform strong shake table tests from multiple directions, such as a nominal case, and cases with directions rotated 45, 60, or 90 degrees. One reason to do this is to test the symmetry of the system response, but also because the starting location of the fuel assemblies inside the basket is expected to change each time.

## 7.2 Horizontal Cask Tip-Over Evaluation

The NUHOMS® AHSM-HS unit was evaluated for potential tip-over using the model shown in Figure 21 and the seismic motion developed in Section 4. A relatively small friction coefficient of 0.2 was used to represent a lower bound threshold for realistic steel to concrete friction. The strongest earthquake horizontal direction was aligned with the X Cartesian direction in the model, which is parallel to the long

axis of the canister. The response of the horizontal cask system was to follow the motion of the pad with a negligible amount of sliding. There was no discernable lift-up or tilt in the horizontal system.

The seismic response is best summarized by the X-direction velocity of each of the 32 fuel assemblies, as shown in Figure 35. The first 0.2 seconds of model time represent a settling period under gravity loading. Each fuel assembly begins the analysis centered in the basket and falls a few millimeters to come to rest in contact with the basket. Unlike the vertical cask scenario, all fuel assemblies experience the same motion.

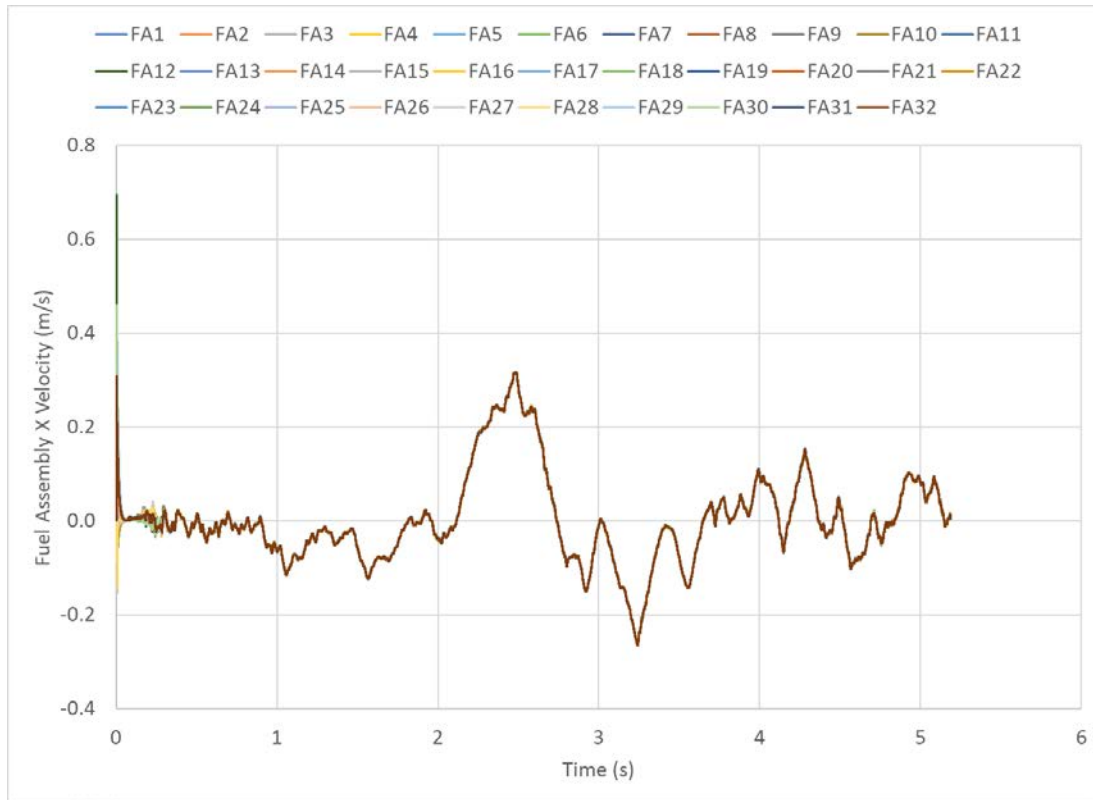


**Figure 35. Fuel Assembly Seismic Response in Horizontal Cask System**

The conclusion drawn from the horizontal cask response is that the potential for tipover is very low. We will need to perform pretest predictions based on the actual shake table input that will be provided by SC Solutions, but at present there is no apparent need to construct a stabilizer system for the horizontal configuration to keep it from tipping over. One feature of the final shake table motion that might affect the tipover potential is rotational shake table motion. The working seismic time histories were developed with translational components only. All rotations are assumed to be zero. If significant shake table rotations are present, they could make tipover a more serious concern.

This page is intentionally left blank.

## 8. CRACK PROPAGATION MODELING

PNNL continued the development of a crack propagation model that was first proposed in the cumulative effects analysis framework report (Klymyshyn et al. 2020b) that was completed earlier this fiscal year. A crack propagation model is needed to estimate the potential for cracks to grow in response to external transient loading events, such as a cask system experiencing a seismic event. This crack propagation model is first being developed for use in evaluating crack growth in stainless steel SNF canisters, then its application to SNF cladding and other fuel assembly components will be evaluated. This topic is directly related to the seismic test plan because the pre-test predictions and the test data will be used as analysis cases for the crack propagation model. Note that the focus of the seismic testing is the fuel assembly response and collecting test data specifically for the crack propagation modeling task is not a priority of the test campaign. Crack propagation modeling is a separate effort that will make use of any seismic test data that happens to be useful.

### 8.1 Crack Propagation Model Setup

Predicting crack growth and subsequent failure of a multipurpose canister (MPC) is imperative for quantifying the structural integrity of MPCs during storage, transport, or an unforeseen loading event. A robust high-fidelity fatigue crack propagation model has been developed to predict the final crack depth in MPCs subjected to a series of random loading events. The crack propagation model will be able to predict final crack depth in every metallic section of the MPC. This model will aid in outlining critical locations within the MPC that are prone to fatigue failure. Due to the long storage times and possible unknown loading history of these MPCs, a damage tolerance approach is taken in which it is assumed that preexisting cracks or flaws are present within the component. The crack growth model described in detail below is able to use finite element analysis data to predict locations within the MPCs that will experience significant crack growth resulting in the depreciation of the structural integrity of the MPC.

Three distinct and experimentally observed stages of fatigue damage are represented by Equation (1):

$$N_{Total} = N_{inc} + N_{SC} + N_{LC} \quad (1)$$

where

- $N_{Total}$  = the total number of cycles to failure,
- $N_{inc}$  = the number of cycles to incubate a crack,
- $N_{SC}$  = the number of cycles in the small crack growth regime, and
- $N_{LC}$  = the number of cycles for the long crack regime.

Due to a damage tolerance approach being applied and an assumed preexisting crack, the incubation portion of the model is not required and therefore only the small crack growth and long crack growth regimes will be accounted for. Figure 37 (at the end of this subsection) shows a standard crack growth rate curve for a given material. A crack growth rate curve is classified into three stages, labeled 1, 2, and 3. Stage 1 is the small crack growth regime, and will be modeled based on the crack tip opening displacement equation Equation (2) developed by McDowell et al. (2003).

$$\left(\frac{da}{dN}\right)_{SC} = \chi(\Delta CTD - \Delta CTD_{th}) \quad (2)$$

where,  $\Delta CTD_{th}$  is the crack tip displacement threshold,  $\Delta CTD$  is the crack tip opening displacement range, and  $\chi$  is a material constant that signifies crack tip irreversibility for a given material. The crack tip opening displacement threshold ( $\Delta CTD_{th}$ ) is equivalent to the Burger's vector for the given material. The crack tip opening displacement range, given by Equation (3), is separated to account for low cycle and high cycle fatigue.

$$\Delta CTD = C_{II} \left( \frac{GS}{GS_0} \right)^\omega \left( \frac{GO}{GO_0} \right)^{\overline{\omega}} \left[ \frac{U\Delta\hat{\sigma}}{S_{ut}} \right]^\zeta a_i + C_I \left( \frac{GS}{GS_0} \right)^\omega \left( \frac{GO}{GO_0} \right)^{\overline{\omega}} \left( \frac{\Delta\gamma_{max}^p}{2} \right)^2 \quad (3)$$

where,

$C_I$  = represents the low cycle fatigue coefficient,

$C_{II}$  and  $\zeta$  = material constants for the high cycle fatigue regime,

$S_{ut}$  = the monotonic ultimate tensile strength, and

$a_i$  = the initial crack length.

$GS$ ,  $GS_0$ ,  $GO$ ,  $GO_0$ ,  $\omega$ , and  $\overline{\omega}$  are grain size and orientation material constants. The equivalent uniaxial stress amplitude,  $\Delta\hat{\sigma} = 2\theta\bar{\sigma}_a + (1d\theta)\Delta\sigma_1$ , is defined as the linear combination of effective stress

amplitude,  $\bar{\sigma}_a = \sqrt{\frac{3}{2} \frac{\Delta\sigma'_{ij}}{2} \frac{\Delta\sigma'_{ij}}{2}}$ , and the maximum principal stress range  $\Delta\sigma_1$ . The coefficient U is used to

model the mean stress effects pertaining to crack growth, where  $U = \frac{1}{1-R}$  is for the case when  $R \leq 0$  and  $U = 1$  for  $R > 0$ . The small crack portion of the model is calibrated to fit a given materials microstructural features and fatigue life curves for a variety of strain amplitudes.

The small crack growth portion of the model for SS316 was calibrated using small crack growth data generated by Vasek et al. (1996). Due to a lack of available data in the literature for small crack growth of SS304, the same parameters generated for SS316 will be used.

Once the crack has grown to several millimeters in length, the crack will be in the long crack growth regime, which is represented by Stage 2 in Figure 37. Long crack growth will be captured using traditional linear elastic fracture mechanics. Traditional Stage 2 growth is represented by the Paris (Paris et al. 1999) equation, Equation (4):

$$\left( \frac{da}{dN} \right)_{LC} = C_0 \Delta K^n \quad (4)$$

However, the Paris equation assumes a constant stress ratio. Because of variable amplitude loading applied to the MPCs the stress ratio is not constant. Therefore, to account for the change in stress ratio the Walker (1970) equation must be implemented (Equation (5)).

$$\left( \frac{da}{dN} \right)_{LC} = \frac{C_0}{(1-R)^{n(1-\gamma)}} * \Delta K^n \quad (5)$$

The Walker equation is similar to the Paris equation, except that the value  $C_0$  is the intercept constant at stress ratio (R) equal to zero.  $\gamma$  is the material constant representing how much the stress ratio affects crack growth. The stress intensity range ( $\Delta K$ ) is given by Equation (6).

$$\Delta K = Y\Delta\sigma\sqrt{\pi a} \quad (6)$$

where Y is a dimensionless geometry factor dependent on geometry of the crack, geometry of the component, and loading configuration, and  $a$  is the crack size. For this work a cylindrical component geometry (Figure 36) is assumed and is given by Eq. 7-10. The geometry factor would change based on the geometry of the component being used in the model.

$$Y = G * G_1 \quad (7)$$

$$G = 0.92 * \frac{2}{\pi} * \sec(B) * \left( \frac{\tan(B)}{B} \right)^2 \quad (8)$$

$$G_1 = 0.752 + 1.286B + 0.37 * [1 - \sin(B)]^2 \quad (9)$$

$$B = \frac{2}{\pi} * \frac{a}{D} \quad (10)$$

where  $a$  is the crack depth and  $D$  is the diameter of the cylindrical component.

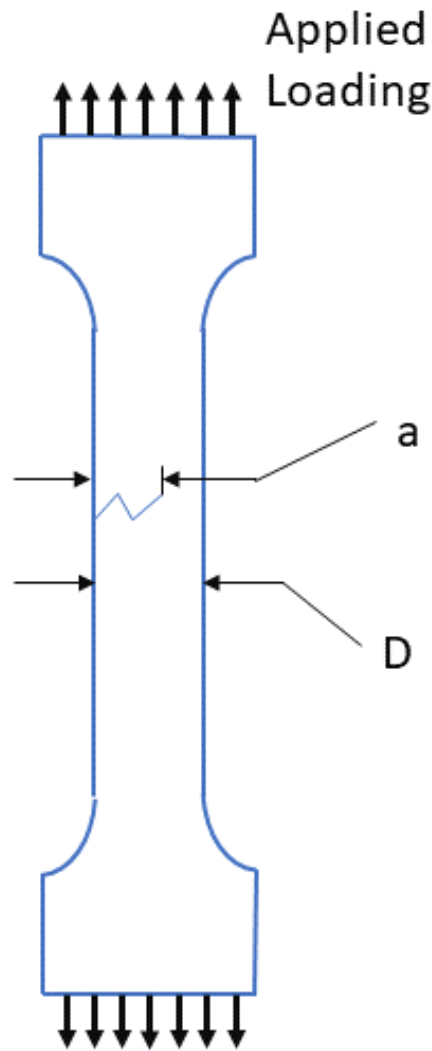


**Figure 36. Schematic of a Cylindrical Fatigue Specimen Used in this Model. Where  $a$  is crack depth and  $D$  is the diameter of the gauge section of the specimen.**

The long crack growth portion of the model for SS304 was calibrated using data generated at PNNL and SS316 was calibrated using data generated by Sajith et al. (2019).

The transition from the small crack growth regime (Stage 1) to the long crack growth regime (Stage 2), shown in Figure 37, is determined by if Eq. 2 or Eq. 4 produces the higher crack growth rate. For example, for a given iteration if the small crack growth rate given by Eq. 2 is larger than the value given long crack growth rate (Eq.4) then the crack propagation model is governed by the small crack growth equations. However, if the long crack growth rate given by Eq. 4 is larger than the value given by Eq. 2 then the crack propagation model is governed by the long crack growth equations. Once  $\Delta K$  exceeds the critical stress intensity factor ( $K_c$ ), the crack fails.

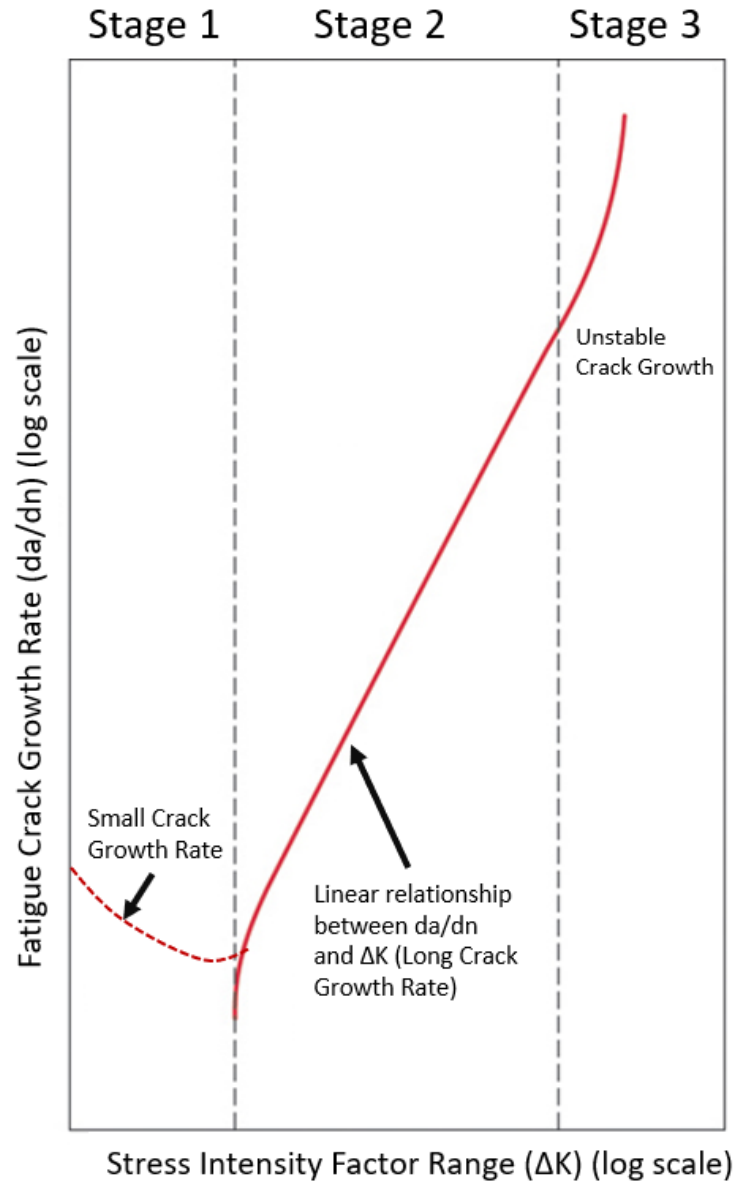


**Figure 37. Crack Growth Rate as a Function of Stress Intensity Factor Range for a Material. This is categorized into three stages of crack growth, small crack growth, and long crack growth and unstable crack growth**

### 8.1.1 Crack Propagation Model Calibration

Figure 38 shows the small crack growth rate of SS316 versus crack length for experiments compared to the small crack growth portion of the model. The model slightly overpredicts the crack growth rate compared to the experimental results because of the minimal amount of data available in the literature. However, the long crack portion of the model is in good correlation with the experimental results (Figure 39A and B).

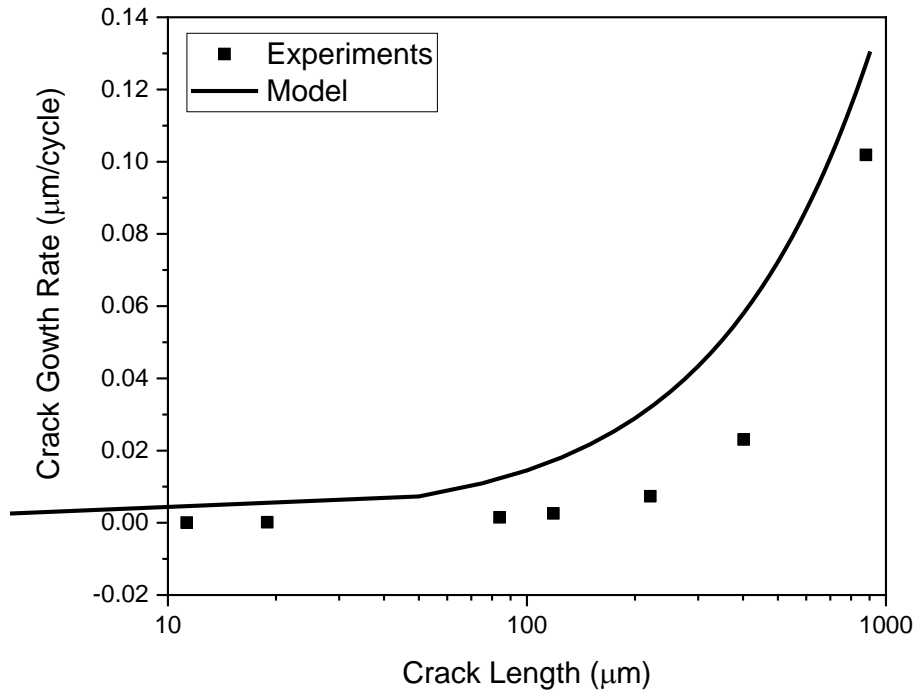


Figure 38. Comparison between the Model and Experiments (Vasek et al. 2003) for Small Crack Growth Rate as a Function of Crack Length for SS316

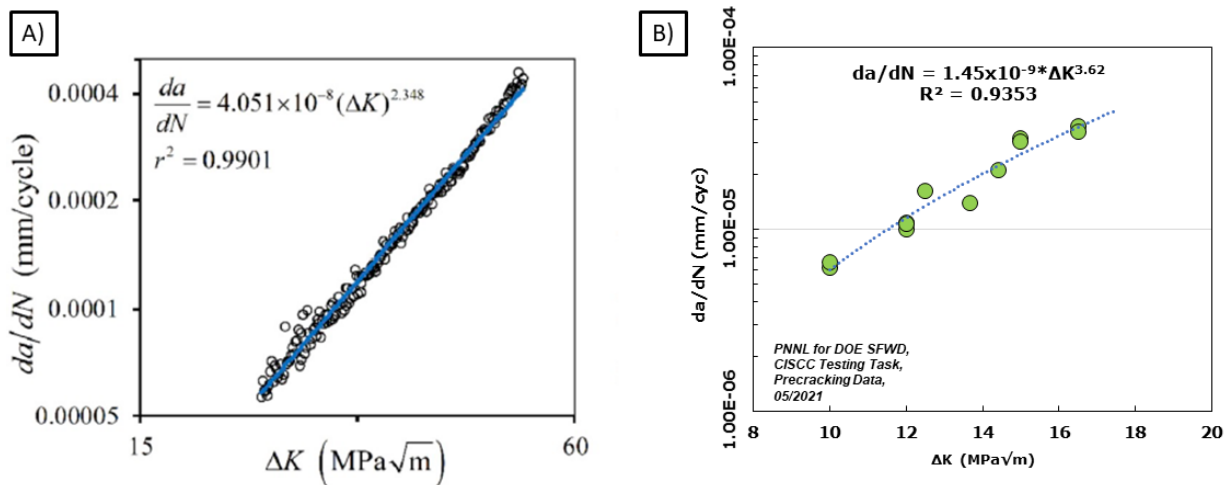
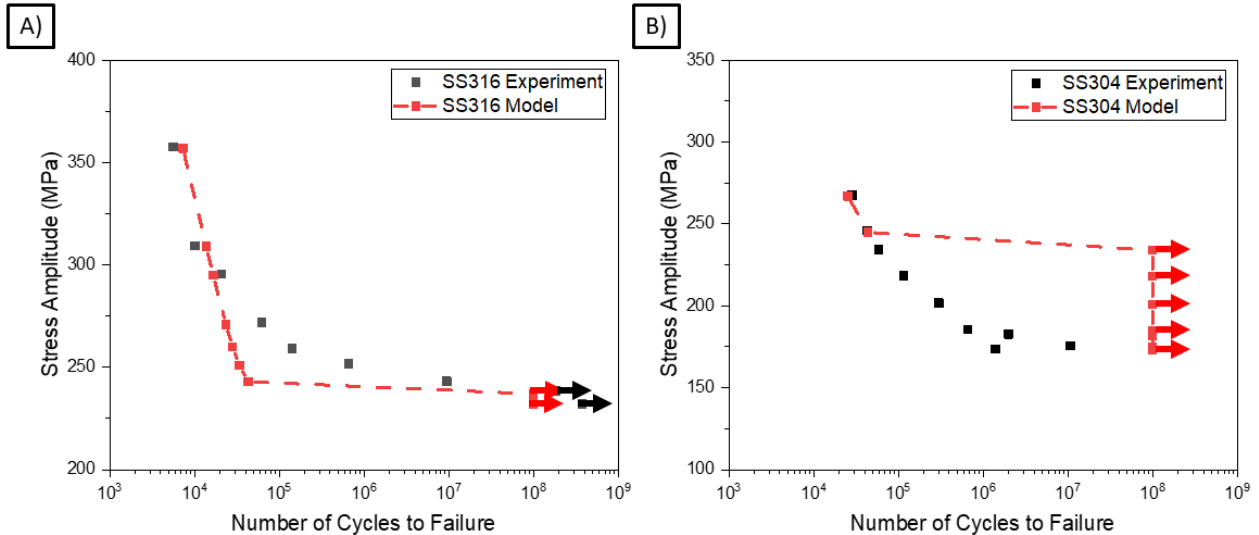


Figure 39.  $da/dN$  vs.  $\Delta K$  Curves Used to Calibrate the Long Crack Growth Portion of the Model for A) SS316 (Sajith et al. 2019) and B) SS304

Figure 40 displays a S-N curve comparison between the crack propagation model and experimental data for SS316 and SS304. The arrows represent an infinite fatigue life at the given values. For the higher stress amplitudes (greater than ~280 MPa) the crack propagation model correlates well with the experimental data. However, for stress amplitudes less than ~280 MPa but above the stress amplitude that generates a stress intensity above the threshold K value, the crack propagation model does not correlate well to the experimental data. The reason for this is because the crack propagation model assumes that there is already a crack present within the material however the experimental study is on smooth fatigue specimens where there is not an initial crack present. Fatigue failure at higher stress

amplitudes is dominated by short and long crack growth, while lower strain amplitudes are dominated by cycles till crack initiation and small crack growth. There was a minimal amount of short crack growth data for both SS316 and SS304. Future fatigue experiments, similar to that outlined by Cauthen et al. (2020), must be conducted in order to properly calibrate the small crack portion of the model. A crack initiation portion of the model could also be added in order to better correlate to experimental results.



**Figure 40. A S-N Curve Comparison between Experimental and Crack Propagation Model Prediction for A) SS316 and B) SS304. The arrows indicate infinite fatigue life.**

### 8.1.2 Example of Model Capabilities

Figure 41 shows model results for two different variable loading conditions for SS316, where the failure criterion is a stress intensity exceeding  $50 \text{ MPa}\sqrt{\text{m}}$  exhibited at the crack tip. The Variable 1 loading condition exhibits a fully reversed stress amplitude of 350 MPa for ~1500 cycles, then a fully reversed stress amplitude of 30 MPa for an additional 35,000 cycles, and then a fully reversed stress amplitude of 245 MPa until failure occurs. The Variable 2 loading condition mimics random variable loading that could be expected during a seismic event. The random loading condition is generated by creating an array of random stress value generated between -550 MPa and 550 MPa. This will mimic the stress exhibited within a given location of the MPCs. Then a rainflow cycle counter converts the random stress into a categorized series of stress amplitudes. Figure 41A plots crack length as a function of cycles for the Variable 1 loading condition. The model is able to account for shifts in stress amplitude as evident in the shifts in crack growth rate exhibited in Figure 41A. The crack length does not grow when the applied crack tip stress intensity factor,  $K$ , is below the threshold  $K$  value for crack growth. Figure 41C shows the stress intensity range at the crack tip as a function of cycles for the Variable 1 loading condition. The shift in stress intensity range trend correlates to the shift in applied stress amplitude. Figure 41B plots crack length as a function of cycles for the Variable 2 loading condition. At first glance there appears to be steady crack growth despite random stress amplitudes being applied. However, Figure 41D shows that for each given cycle the stress intensity range changes with each different applied stress amplitude. This indicates that the model is capable of predicting crack length with variable randomized loading conditions that one would expect to be applied to MPCs during seismic loading events.

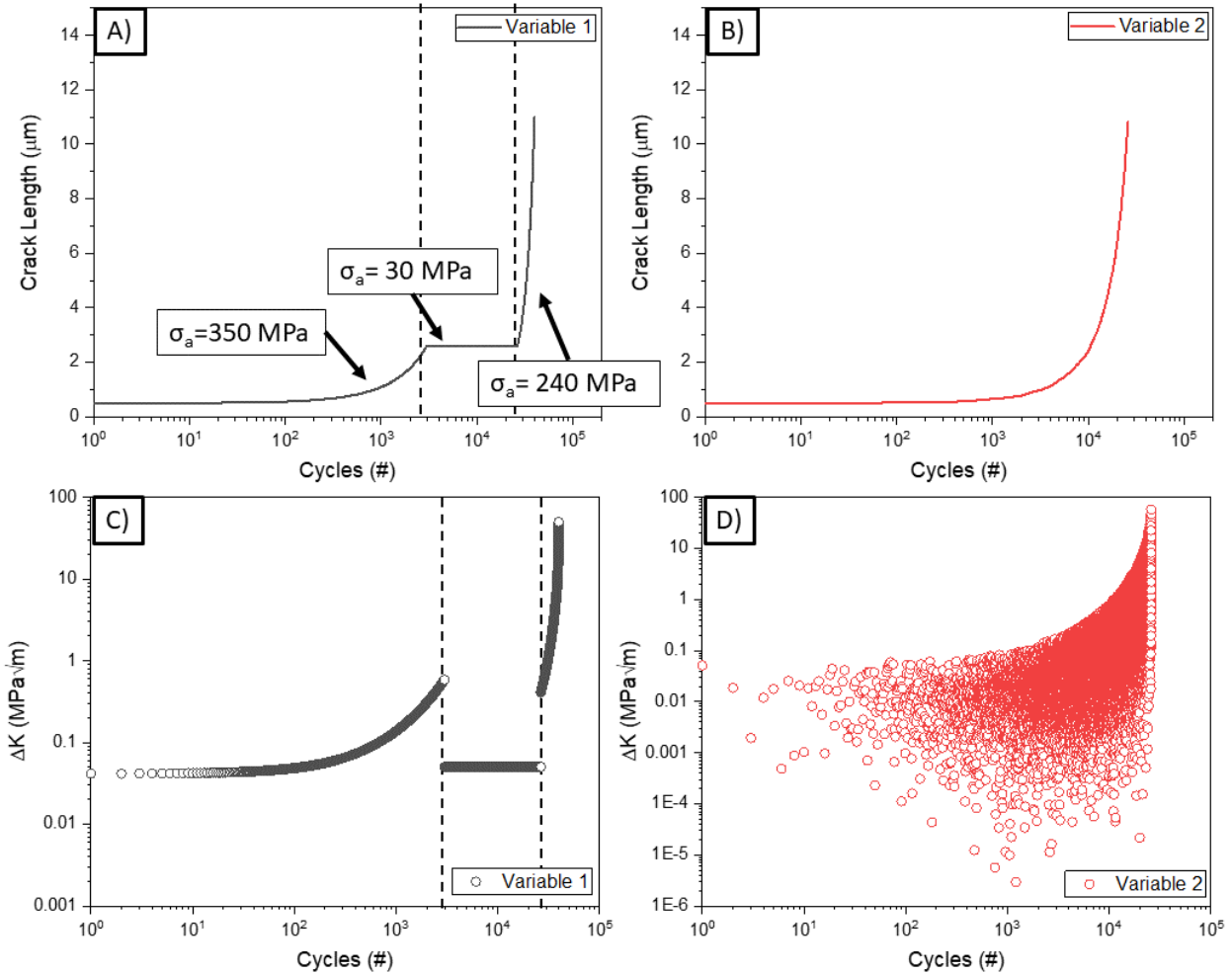


**Figure 41. Crack Propagation Model Prediction for Two Different Loading Conditions for SS316. A) Crack length as a function of cycles for the Variable 1 loading condition. B) Crack length as a function of cycles for the Variable 2 loading condition. C) Stress intensity range as a function of cycles for the Variable 1 loading condition. D) Stress intensity range as a function of cycles for the Variable 2 loading condition.**

## 8.2 Crack Propagation Modeling Summary and Future Work

A crack propagation model was developed to predict crack growth in MPCs subjected to variable loading conditions. The crack propagation model was able to account for randomized loading conditions applied to the model. The long crack growth portion of the model correlated well with experimental results. However, future work needs to be conducted to produce experimental fatigue data for both SS316 and SS304 in order to accurately capture the small crack growth regime.

This page is intentionally left blank.

## 9. CONCLUSIONS AND NEXT STEPS

This report summarizes the modeling, analysis, and test plan support completed by PNNL in support of the SNF dry storage system seismic test plan through May of 2021.

PNNL started hardware design efforts to provide the project engineering drawings to find fabricators and cost estimates for the vertical concrete cask system. PNNL also generated a first estimate dummy fuel assembly design, based on Spanish and Korean examples. Both the vertical cask design and the dummy assembly design will be updated as the test details become finalized.

PNNL generated a hypothetical ground motion for use in developing the finite element models. The ground motion used in the current models is based on the earthquake motion at the base rock level at the Columbia Generating Station in Washington State. The ground motion applied to the cask models includes accelerations in the magnitude and dynamic frequency ranges that are typical of a strong seismic event. Note that SC Solutions is tasked to provide the final ground motion data for analysis and shake table testing in this project. The current model results will be reassessed when those seismic inputs are available. The focus of future efforts will be on preparing pre-test predictions for the shake test.

The structural dynamic modeling of cask systems led to the following key conclusions:

- The fuel assembly loads are expected to vary throughout the canister in the vertical storage system but are expected to be nearly uniform in the horizontal system.
- Mixing fuel assembly designs with different geometries and gap conditions is not a problem for the test. In the case of the vertical canister configuration, a variation of fuel assembly response is expected, and mixing fuel assembly designs is expected to have effects that are within that natural variation. In the case of the horizontal canister configuration, the response of all fuel assemblies is approximately uniform and they all match the motion of the canister. Mixing fuel assemblies in the horizontal case is not expected to have any significant effect because the response range is linear.
- It is recommended that selected strong shake table cases for the vertical canister case be repeated at different orientation angles in the horizontal plane, such as 0°, 45°, and 90°. The response is expected to be similar in all cases, but the initial relative locations of the fuel assemblies are expected to have an influence on the fuel assembly mechanical response. The goal of such repeated tests is to establish the range of response of the fuel assemblies to the same applied motion.

The fuel assembly modeling led to 3 key conclusions:

- The mechanical loading environment for fuel assemblies may be similar to the 30 cm cask drop case, with the exception that grids are not expected to buckle or to experience significant permanent deformation. The current model predicts maximum permanent grid deformation values below 0.1 mm for the assumed loading condition. It remains to be determined whether the shake table motion of the test will be strong enough to cause minor fuel assembly grid spacer permanent deformation or if the grid impact response will remain elastic.
- The seismic fuel assembly loads for the strongest earthquakes to be considered during the test are expected to be significantly stronger than the MMTT, comparable to the cask side drop 30 cm drop test data, but weaker than the maximum potential loads estimated through modeling for the general 30 cm cask drop scenario.
- The seismic fuel assembly loads for the weakest earthquakes to be considered during the test were not evaluated, but the ground motion accelerations are expected to be about 10 times lower in intensity. This reduction in ground motion intensity is expected to reduce the loads

substantially, although the nonlinear response in the vertical canister case makes it impossible to predict the extent of the load reduction without running comparison cases.

The development of a crack propagation model continued in parallel with the seismic test plan preparation. The crack propagation model used test data from PNNL's chloride-induced stress corrosion cracking testing effort to calibrate the model, and the test data from the seismic test will be evaluated using the model to determine if crack propagation is expected. This crack propagation modeling work is not a priority for the seismic test, we are just working to use data available in the SFWST program to achieve cross-project benefits.

## 10. REFERENCES

- Cauthen, C., Anderson, K.V., Avery, D.Z., Baker, A., Williamson, C.J., Daniewicz, S.R., Jordon, J.B., “Fatigue crack nucleation and microstructurally small crack growth mechanisms in high strength aluminum alloys,” *Int. J. Fatigue*, vol. 140, no. February, p. 105790, 2020, doi: 10.1016/j.ijfatigue.2020.105790.
- ISO (International Standards Organization). 2007. Mechanical vibration and shock – Signal processing – Part 4: Shock-response spectrum analysis. ISO 18431-4:2007(E), Geneva, Switzerland.
- Kalinina, E.A., Wright, C., Gordon, N., Saltzstein, S.J., Lujan, L., Norman, K.M. 2018. *Data Analysis of ENSA/DOE Rail Tests*. SFWD-SFWST-2018-000494, Sandia National Laboratories, Albuquerque, New Mexico.
- Kalinina, E., D. Ammerman, C. Grey, G. Flores M, L. Lujan, S. Saltzstein, D. Michel. 2020. “Surrogate Assembly 30 cm Drop Test.” Sandia National Laboratories, Albuquerque NM, 2020.
- Klymyshyn, N.A., Ivanusa, P., Kadooka, K., Spitz, C., Jensen, P.J., Ross, S.B., Hanson, B.D., Garcia, D., Smith, J., Lewis, S. “Modeling and Analysis of the ENSA/DOE Multimodal Transportation Campaign.” PNNL-28088, Pacific Northwest National Laboratory, Richland WA, 2018.
- Klymyshyn N.A., K. Kadooka, P. Ivanusa, C.J. Spitz, and J.F. Fitzpatrick. 2020a. 30 cm Drop Modeling. PNNL-30495. Richland, WA: Pacific Northwest National Laboratory.
- Klymyshyn N.A., B.J. Jensen, C.F. Campbell, C. Mason, K. Kadooka, and J.F. Fitzpatrick. 2020b. Developing an Analytical Framework for Cumulative Effects. PNNL-30647. Richland, WA: Pacific Northwest National Laboratory.
- McConnell, P.E., Ross, S.B., Grey, C.A., Uncapher, W.L., Arviso, M., Garmendia, R., Perez, I.F., Palacio, A., Calleja, G., Garrido, D., Casas, A.R., Garcia, L.G., Chilton, W., Ammerman, D.J., Walz, J., Gershon, S., Saltzstein, S.J., Sorenson, K., Klymyshyn, N.A., Hanson, B.D., Pena, R., Walker, R. 2018. *Rail-Cask Tests: Normal-Conditions-of- Transport Tests of Surrogate PWR Fuel Assemblies in an ENSA ENUN 32P Cask*. SFWD-SFWST-2017-000004, Sandia National Laboratories, Albuquerque, New Mexico.
- McDowell, D.L., K. Gall, M. F. Horstemeyer, and J. Fan, “Microstructure-based fatigue modeling of cast A356-T6 alloy,” *Eng. Fract. Mech.*, vol. 70, no. 1, pp. 49–80, 2003, doi: 10.1016/S0013-7944(02)00021-8.
- NRC (U.S. Nuclear Regulatory Commission). 2005. *Parametric Evaluation of Seismic Behavior of Freestanding Spent Fuel Dry Cask Storage Systems*. NUREG/CR-6865, SAND2004-5794P, NUREG/CR-6865, prepared for Division of Engineering Technology Office of Nuclear Regulatory Research U.S. Nuclear Regulatory Commission by Sandia National Laboratories (and collaborators), Albuquerque, New Mexico.
- Paris, P.C., H. Tada, and J. K. Donald, “Service load fatigue damage - A historical perspective,” *Int. J. Fatigue*, vol. 21, no. SUPPL. 1, pp. 35–46, 1999, doi: 10.1016/s0142-1123(99)00054-7.
- Sajith, S., S. S. Shukla, K. S. R. K. Murthy, and P. S. Robi, “Mixed mode fatigue crack growth studies in AISI 316 stainless steel,” *Eur. J. Mech. A/Solids*, vol. 80, no. November 2019, p. 103898, 2020, doi: 10.1016/j.euromechsol.2019.103898.
- Vašek, A., J. Polák, and K. Obrtlík, “Fatigue damage in two-step loading of 316L steel II. Short crack growth,” *Fatigue Fract. Eng. Mater. Struct.*, vol. 19, no. 2, pp. 157–163, 1996, doi: 10.1111/j.1460-2695.1996.tb00955.x.

Walker, K. “The Effect of Stress Ratio During Crack Propagation and Fatigue for 2024-T3 and 7075-T6 Aluminum,” in *Effects of Environment and Complex Load History on Fatigue Life*, 100 Barr Harbor Drive, PO Box C700, West Conshohocken, PA 19428-2959: ASTM International, 1970, pp. 1-1–14.